VE-Mobicast: A Variant-Egg-Based Mobicast Routing Protocol for Sensornets

YUH-SHYAN CHEN*, SHIN-YI ANN, and YUN-WEI LIN

Department of Computer Science and Information Engineering, National Chung Cheng University

Chiayi 621, Taiwan, R.O.C.

Abstract

In this paper, we present a new "spatiotemporal multicast", called a "mobicast", protocol for supporting applications which require spatiotemporal coordination in sensornets. The spatiotemporal character of a mobicast is to forward a mobicast message to all sensor nodes that will be present at time t in some geographic zone (called the forwarding zone) Z, where both the location and shape of the forwarding zone are a function of time over some interval (t_{start}, t_{end}). The mobicast is constructed of a series of forwarding zones over different intervals (t_{start}, t_{end}), and only sensor nodes located in the forwarding zone in the time interval (t_{start}, t_{end}) should be awake in order to save power and extend the network lifetime. Existing protocols for a spatiotemporal variant of a multicast system were designed to support a forwarding zone that moves at a constant velocity, $\overrightarrow{v}$, in sensornets. To consider the path of a mobile entity which includes turns, this work mainly develops a new mobicast routing protocol, called the variant-egg-based mobicast (VE-mobicast) routing protocol, by utilizing the adaptive variant-egg shape of the forwarding zone to achieve high predictive accuracy. To illustrate the performance achievement, a mathematical analysis is conducted and simulation results are examined.

Keywords: Sensornet, wireless communication, mobile computing, mobicast, routing, distribution.

1 Introduction

Sensornets [1] are large-scale distributed embedded systems composed of a large number of small-sized, low-cost, low-power devices that integrate sensors, actuators, wireless communication technologies, and microprocessors. In sensornets, sensor nodes can be set up in hazardous or faraway environments due to their disposable capability. Energy is a scarce resource in sensornets, and so it has

*Corresponding author. E-mail: yschen@cs.ccu.edu.tw

to be wisely managed to extend the sensornet lifetime. Many techniques have been investigated for their power-saving properties for sensornets, such as energy-efficient MAC protocols [17][22][24], self-organization schemes [16][25][26], a distributed clustering approach [31], a directed-diffusion protocol [13], energy-efficient routing protocols [9][20][21][23][32], and new sensornet applications, such as object tracking [8][27][30], human body and environmental monitoring [2][6], etc. In these sensornet applications, a sink node collects aggregated data from many sensor nodes. Data aggregation is often driven by the locality of environmental events and entails coordination of activities subject to spatial constraints. Information about the environmental event is more relevant to users close to where the event is taking place than to those farther away. Many important sensor network applications (e.g., habitat monitoring [2][6], intruder detection [19], and object tracking [8][27][30]), involve monitoring mobile physical entities that move in sensornets. To save power, only sensors close to the physical entity of interest should participate in data aggregation. To continuously monitor a mobile entity, a sensor network must maintain an active sensor group that moves at the same velocity and along the same path as the physical entity. Achieving energy efficiency requires two operations [10][11][12]. The first operation is to activate and deactivate sensors as required. Only a small number of sensors need to be active in order to provide continuous coverage so that energy is not wasted. The second operation is to actively move information about a known physical entity to other sensors before that entity arrives in their vicinity, by waking up sleeping sensors at the appropriate time for better monitoring and action.

A new multicast communication paradigm called a ”spatiotemporal multicast” or ”mobicast” was recently investigated in [10][11][12] which supports spatiotemporal coordination in applications over wireless sensor networks. The distinctive feature of this new form of multicast is the delivery of information to all nodes that happen to be in a prescribed region of space at a particular point in time. This prescribed region is a geographic zone and is denoted the *forwarding zone* in this study. The set of multicast message recipients is specified by a forwarding zone which continuously moves and evolves over time. When continuously monitoring a mobile entity, forwarding zones at different time intervals greatly differ. This provides a mechanism for application developers to express their needs

for spatial and temporal information dissemination directly to the multicast communication layer. This study was motivated by the need to predict and determine the right shape, size, and location of the forwarding zone at the right time in order to wake up the least number of sleeping sensor nodes. This offers a new just-in-time multicast delivery paradigm. In this paper, the *predictive accuracy* of the forwarding zone is the key performance metric for designing an energy-efficient mobicast routing protocol. The predictive accuracy is used to reflect the status of determining the right shape, size, and location of the forwarding zone at the appropriate time. The more accurate the predictive accuracy is, the more power that will be saved. Efforts are made in this paper to develop a new mobicast routing protocol with a high predictive accuracy.

Existing protocols for a spatiotemporal variant of a multicast system called a "mobicast" were designed to support a forwarding zone that moves at a constant velocity, $\overrightarrow{v}$, in the sensornet. To consider the path of a mobile entity which makes a turn, we have developed a new adaptive mobicast routing protocol called the variant-egg-based mobicast (VE-mobicast) routing protocol, which utilizes the adaptive variant-egg shape of the forwarding zone to achieve mobicast forwarding with a high predictive accuracy. The main features of our VE-mobicast routing protocol are summarized as follows: (1) the VE-mobicast protocol creates a new adaptive and dynamic shape of the forwarding zone, called the variant-egg, to adaptively determine its size, shape, and location of the forwarding zone such that the least number of sensor nodes are woken up; (2) the VE-mobicast protocol is a fully distributed algorithm to effectively reduce the communication overhead of constructing the forwarding zone and the that of mobicast message forwarding; (3) the VE-mobicast routing protocol offers high predictive accuracy of the forwarding zones.

The rest of this paper is organized as follows. Section 2 discusses related work. Section 3 describes the basic ideas and design challenges. Our proposed VE-mobicast protocol is presented in section 4. To illustrate the performance achievement, a mathematical analysis is conducted and simulation results are examined in Section 5. Finally, section 6 concludes this paper.

2 Related work

This paper focuses on developing power-aware routing protocols to support many various sensornet applications. The main existing power-aware routing schemes are introduced as follows. Gao *et al.* [9] proposed an adaptive network/routing algorithm for energy-efficient cooperative signal processing in sensornets. This algorithm offers a distributed selection procedure to produce a fewer number of winners, and only winners need to provide raw data; therefore energy is saved. Youssef *et al.* [32] proposed an energy-aware routing protocol to minimize energy consumption, and their work also maintained better end-to-end delay, throughput, and system performance. In addition, multicast routing is an important communication pattern in mobile ad hoc networks (MANETs) and sensornets to send the same message to a set of destination nodes and receive aggregated data from a set of nodes. Many multicast routing protocols [20][21][23] have been developed for MANETs. For example, Maleki *et al.* [20] presented a lifetime-aware multicast routing algorithm to maximize MANET lifetimes. It is important in geocast routing, a special case of multicast routing, in which all destination nodes are within a fixed geographical region. Many novel geocast routing protocols [3][14][15][18] have been investigated for MANETs.

A new ”spatiotemporal multicast” was presented for supporting sensornet applications which require spatiotemporal coordination. The spatiotemporal character of the mobicast is to forward a mobicast message to all nodes that will be present at time t in some geographic zone (called a forwarding zone), F, where both the location and shape of the forwarding zone are a function of time over some interval (t_{start}, t_{end}). The mobicast is constructed by a series of forwarding zones over different intervals (t_{start}, t_{end}), and only sensor nodes located in the forwarding zone in the time interval (t_{start}, t_{end}) are woken up in order to save power. Huang *et al.* recently developed three mobicast routing protocols [10][11][12].

Huang *et al.* [11] initially designed a spatiotemporal multicast protocol for sensornets. They used the *compactness* of the sensornet to determine the size of the forwarding zone. The minimum value of compactness was calculated under the assumption that the global network topology is known [11]; however, the communication overhead of the mobicast protocol is very high. To reduce the

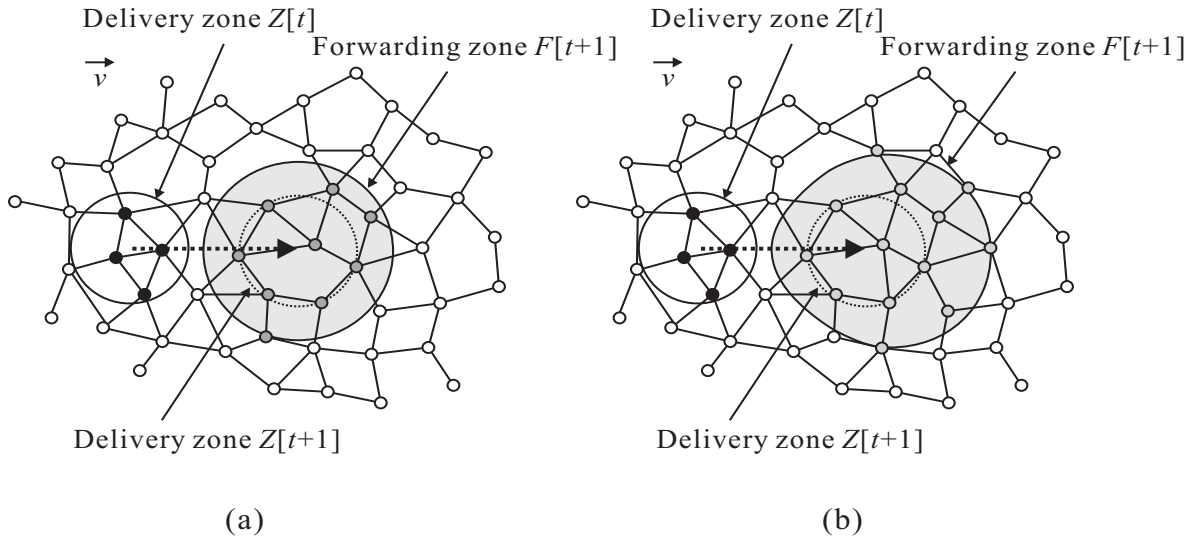

Figure 1: Spatiotemporal multicast and VE-mobicast.

communication overhead, Huang *et al.* [10] then presented a new energy-efficient spatiotemporal multicast for sensornets. In this investigation, the value of compactness was estimated within a distributed environment. More recently, Huang *et al.* [12] developed a quite-new mobicast routing protocol, called face-aware routing (FAR). The FAR protocol is a geometric routing protocol which provides reliable routing results. To achieve the reliability, the FAR protocol must periodically maintain a spatiotemporal neighbor list [12] and thus has a heavy communication overhead. Observe that the face-aware approach originated with Bose *et al.* [5]. They considered the routing problems in ad hoc wireless networks modeled as *unit graphs* (faces) in which nodes are points in the plane, and two nodes can communicate if the distance between them is less than some fixed unit. Bose and Morin [4] described an algorithm for enumerating all the faces, edges, and vertices of a connected embedded planar graph, G, without using marked bits or a stack. Efforts are made in this paper to develop a fully distributed algorithm to increase the reliability and decrease the communication overhead. A high predictive accuracy of the forwarding zone is developed in this investigation to additionally consider a mobile entity's path which includes turns.

3 Preliminaries

3.1 System model

The node capabilities of all sensor nodes, including the mobile physical entities (or mobile sink node), in our work are assumed to know their location information by using GPS (Global Positioning System) or other location information-aided devices [26]. Our approach adaptively determines the forwarding zone based on the location information. Without the location information, the exact forwarding zone cannot be accurately determined. This paper is assumed that all nodes are synchronized. When nodes are not synchronized, the predictive mechanism of our VE-mobicast protocol cannot be correctly performed. This leads to predict the incorrect size and shape of the forwarding zone, and it causes power to be needlessly consumed. In addition, all sensor nodes are homogeneously and randomly deployed in a monitoring area by a random network. This paper is only concerned with a static and irregular topology, i.e., all sensor node locations are fixed and irregular. Finally, the main operation of VE-Mobicast is depended on the control packets to determine the right forwarding zone in a distributed fashion. Therefore, this paper is not investigated the robust problem when VE-Mobicast operation losses of control packets.

3.2 The mobicast framework

A new special case of a ”spatiotemporal multicast” protocol is introduced for supporting applications which require spatiotemporal coordination in sensornets. This spatiotemporal multicast protocol provides sensing applications that need to disseminate the multicast message to the ”right” place (or prescribed zone) at the ”right” time. A spatiotemporal multicast session is specified by $<m, Z[t], T_s, T>$, which is defined in [11], where m is the multicast message, $Z[t]$ describes the expected area of message delivery at time t, and T_s and T are the sending time and duration of the multicast session, respectively. As the delivery zone, $Z[t]$, evolves over time, the set of recipients for m changes as well.

A special case of a spatiotemporal multicast, called a mobicast, was considered in [10][11][12]. The delivery zone is some fixed convex polygon, P, that translates through 2-D space at some con-

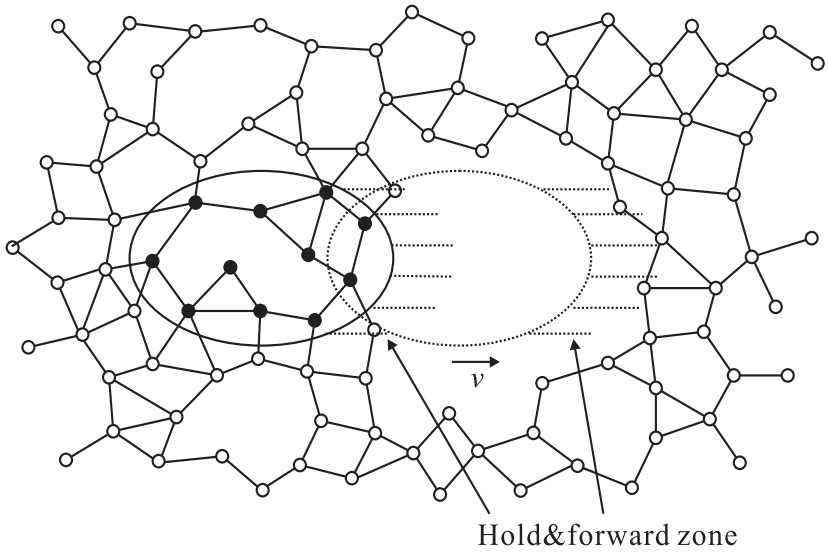

Figure 2: The ”hole” problem in a spatiotemporal mobicast.

stant velocity, $\overrightarrow{v}$ [11]; i.e., $Z[t]$ =$P[\overrightarrow{r_0} + \overrightarrow{v}(t - T_s)]$, with $P[\overrightarrow{r_0}]$ being the polygon centered at $\overrightarrow{r_0}$. Huang *et al.* [10][11][12] called this special class of spatiotemporal multicasts a ”constant velocity mobicast” or ”mobicast”. The polygonal shape of the delivery zone was circular in those papers [10][11][12]. Figure 1(a) shows an example of the delivery zones $Z[t]$ and $Z[t+1]$ for a mobicast.

The mobicast routing protocol is composed of a delivery zone and a forwarding zone. The forwarding zone [11] is comprised of every sensor node in forwarding zone $F[t+1]$ which is responsible for forwarding the mobicast messages in order to guarantee that delivery zone $Z[t+1]$ at time $t+1$ can successfully receive the mobicast message. The size of forwarding zone $F[t+1]$ is always larger than the size of delivery zone $Z[t+1]$. The difference in the forwarding zone using existing mobicast and VE-mobicast routing protocols is compared in figure 1. The shape of a forwarding zone of the existing mobicast routing protocols [10][11][12] is a circle as shown in figure 1(a). The shape of a forwarding zone of our VE-mobicast routing protocol is an oval as illustrated in figure 1(b). The key problem of the mobicast protocol is how to accurately predict the correct size and shape of forwarding zone $F[t+1]$ at time t.

Potential holes in the network show that two nodes which are close in physical space can be relatively far away in terms of network hops [10][11][12]. Many sensor nodes are randomly distributed in a sensornet, so that a sensornet with an irregular topology is constructed. This produces

the ”hole” problem, where a ”hole” is a sensing area with no sensor nodes. This condition always occurs if a ”hole” problem [10][11][12] exists in a sensornet. Figure 2 shows an example of a ”hole” in a spatiotemporal mobicast. Maintaining a large forwarding zone can reduce the ”hole” problem, but it causes power to be consumed needlessly.

Existing mobicast routing protocols are considered ”constant-velocity mobicast”. That is to say, the path of the delivery zones from $Z[t]$ to $Z[t+1]$ is fixed under a constant velocity, $\overrightarrow{v}$. The zone in front of forwarding zone $F[t+1]$ is a ”hold-and-forward” zone where sensor nodes retransmit the mobicast message only after becoming members of the forwarding zone. This behavior results in a ”*hold-and-forward zone*” in front of the forwarding zone, as shown in figure 2. A different path is considered in this work if delivery zone $Z[t]$ moves to $Z[t+1]$ from time t to $t+1$ along a different path and angle. Any forwarding zone, $F[t+1]$, in any existing mobicast routing protocol is unable to guarantee that delivery zone $Z[t+1]$ at time $t+1$ can successfully receive the mobicast message, due to differences in the path which occur from time t to $t+1$. To guarantee reliable delivery, all sensor nodes in forwarding zone $F[t+1]$ must be woken up before delivery zone $Z[t+1]$ reaches the area of $F[t+1]$ at time $t+1$ under a constant velocity, $\overrightarrow{v}$. It is interesting to investigate the condition when all sensor nodes in $F[t+1]$ are already notified to enter the active mode (i.e., to wake up) from sensor nodes in the hold-and-forward zone before time $t+1$. However, if the delivery zone unexpectedly changes its path after time t and before time $t+1$, then it is possible that it will be unable to inform all sensor nodes of $F[t+1]$ in time to enter the power-saving mode before time $t+1$ such that not all sensor nodes of $Z[t+1]$ are in $F[t+1]$. Figure 3(a) shows that some nodes in $Z[t+1]$ are not in $F[t+1]$ when using the mobicast routing protocols in [10][11][12].

The predictive accuracy is defined as the percentage of sensor nodes which are located in both $Z[t+1]$ and $F[t+1]$. If all sensor nodes in $Z[t+1]$ are also in $F[t+1]$, then the predictive accuracy is 100%, while it is 0% if no sensor node of $Z[t+1]$ is in $F[t+1]$. The better the predictive accuracy is, the more power that will be saved. Existing mobicast routing protocols have low predictive accuracies, especially when different paths are considered within the same period of time. Efforts are made in the present study to improve the predictive accuracy by developing a new mobicast routing

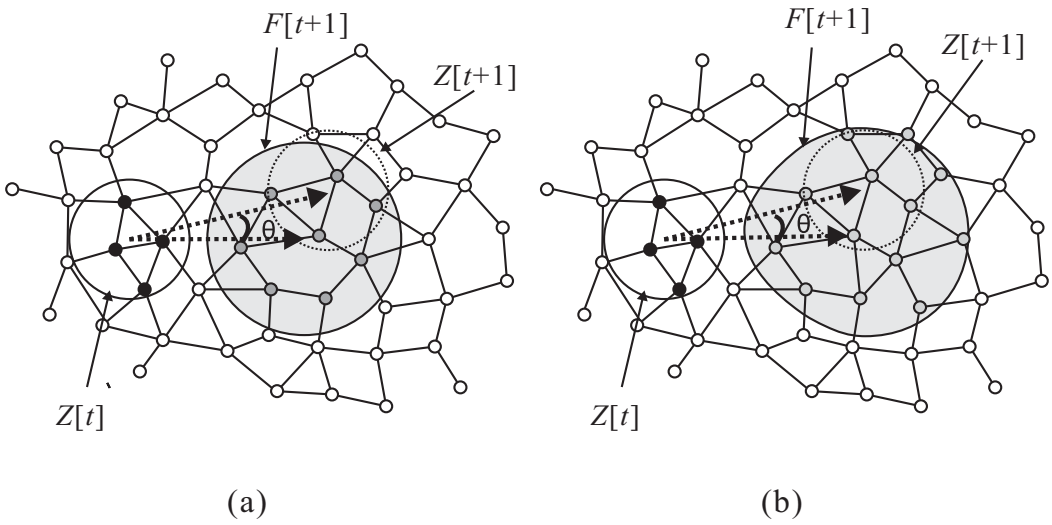

Figure 3: Advantage of a VE-mobicast.

protocol, called the variant-egg-based mobicast (VE-mobicast) routing protocol, which has high predictive accuracy. Consider the same example in figure 3(a), the VE-mobicast routing protocol offers the result of a predictive accuracy of 100% as shown in figure 3(b). This is because our VE-mobicast routing protocol offers the adaptive size and shape of the variant-egg.

3.3 Application examples

There are many interesting and useful applications, such as object tracking [2][27][30] and environmental monitoring [6][8], for sensornets. The mobicast routing protocol can be effectively used for such sensornet applications as intruder tracking and information scouting [10][11][12] as illustrated in figure 4. Figure 4(a) depicts an example of intruder tracking. A set of sensors discovers a tank, and an alert message is sent to all sensor nodes along the intruder's expected path. All sleeping sensor nodes along the intruder's expected path must be woken up to alert and pre-arm them for better tracking and more-sensitive reactions. This alert message can be sent by a mobicast service, using a delivery zone of a desired size that moves at a certain distance ahead of the intruder, with a speed approximating that of the intruder's, thus creating an evolving alert "cloud" immediately in front of it. If the intruder unexpectedly changes its path, then all alert messages along the intruder's former expected path are useless and are wasting power. Extra power is consumed to inform sensor nodes

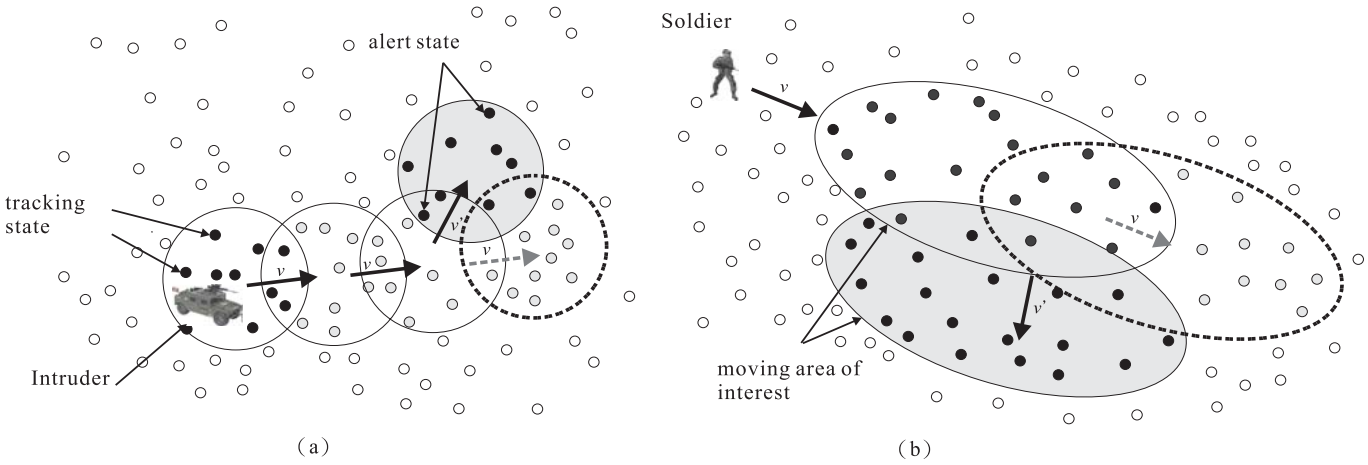

Figure 4: Application examples of the VE-mobicast.

along the intruder's expected path to re-enter the power-saving (PS) mode. This scenario is shown in figure 4(a) if a tank unexpectedly changes its path. This results in some sleeping sensor nodes along the tank's expected path still being woken up in anticipation of the approaching tank.

Figure 4(b) gives another example of information scouting. A soldier is moving toward a fixed area. For safety and action efficiency, the soldier would like to know the field information ahead on his/her path, so he/she can properly adjust to the situation. The area of interest changes in front of him/her as he/she runs forward. Only the sensors that enter the delivery zone will pool their currently sensed information and send aggregated data back to him/her. As illustrated in figure 4(b), if the solider unexpectedly changes direction, then the problem of unnecessarily wasting power of the sensornets occurs. To consider a path with a turn, we have developed a new mobicast routing protocol with a more-accurate predictive accuracy to reduce power consumption and extend sensornet lifetime.

3.4 VE-mobicast in sensornets

The main idea of the VE-mobicast is to develop a distributed and adaptive scheme to provide a dynamic shape of forwarding zone $F[t+1]$ which depends on the actual network topology. From time t to $t+1$, all sensor nodes in $F[t+1]$ should be woken up to guarantee that $Z[t+1]$ is completely in $F[t+1]$ when delivery zone $Z[t]$ moves to $Z[t+1]$. The size and shape of forwarding zone $F[t]$

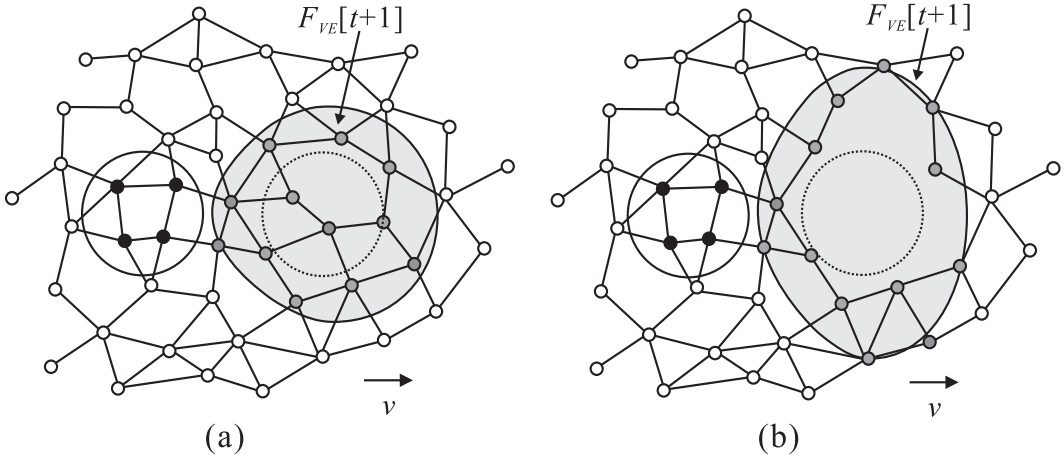

Figure 5: Different forwarding zones of $F_{VE}[t+1]$.

at time t affect the system performance and energy-saving factors for developing a new mobicast routing protocol. In this work, we mainly discuss the effects of the new dynamic shape of the forwarding zone. Maintaining the same number of awake sensor nodes in the dynamic shape of forwarding zone $F[t]$ is the main goal of this work as well as promoting the predictive accuracy when a variable direction of movement is considered. In this paper, delivery zone $Z[t]$ is some fixed polygon, P, that translates through a 2-D space at some constant velocity, $\overrightarrow{v}$, and moving angle, θ, i.e.,

$$Z[t] = P[\overrightarrow{X_0} + \overrightarrow{v}(t - Ts) * \cos\theta, \overrightarrow{Y_0} + \overrightarrow{v}(t - Ts) * \sin\theta], \tag{1}$$

with the polygon center at $P[\overrightarrow{X_0}, \overrightarrow{Y_0}]$. In this investigation, a polygonal shape is adopted for the *delivery zone* instead of a circular shape [10]. In our variant-egg-based scheme, the shape of forwarding zone $F[i]$ at time i is a variant egg, which is denoted by F_{VE} or $F_{VE}[i]$ in this work, where $0 \leq i$. Given a fixed speed of $\overrightarrow{v}$, the size and shape of F_{VE} are determined by the factors of sensornet density and topology. A mobile entity cannot know the sensornet density and topology before it reaches a new location. Therefore, the "hole" problem must effectively be solved for the mobicast. The adaptive and dynamic shape and size of F_{VE} is very useful for overcoming the "hole" problem in sensornets. Figure 5(a) shows a normal size of $F_{VE}[t+1]$ under a normal sensornet density. But if the sensornet density is low and has a "hole" problem, the size of $F_{VE}[t+1]$ is enlarged as shown in

figure 5(b). Developing a new distributed mobicast routing protocol to effectively solve the ”hole” problem is the main objective of this work.

4 VE-mobicast: a variant-egg-based mobicast routing protocol

We first give an overview of our variant-egg-based mobicast (VE-mobicast) routing protocol. The main function of the VE-mobicast routing protocol is to dynamically construct a variant-egg during mobicast operation. The VE-mobicast is divided into two phases. Sensor nodes in a forwarding zone retransmit the mobicast message as soon as they receive it, and the sensor nodes in front of the forwarding zone enter a ”hold-and-forward” state whenever they receive a mobicast message [10][11][12]. They then retransmit the mobicast message only after becoming members of the forwarding zone. This area is denoted the hold-and-forward zone, $H[t]$, at time t. In our VE-mobicast approach, hold-and-forward zone $H[t] = F_{VE}[t] \cap F_{VE}[t+1]$. An example of hold-and-forward zone $H[t]$ is given in figure 6(b).

(1) **Egg estimation** phase: The size of the variant-egg forwarding zone, $F_{VE}[t+1]$, at time t is estimated by sensor nodes in $H[t]$. The forwarding zone [10][11][12] limits retransmission to a bounded space while ensuring that all sensor nodes that need to receive the mobicast message do so.

(2) **Distributed variant-egg-based mobicast** phase: With the estimated $F_{VE}[t+1]$, a distributed algorithm of VE-mobicast operation is presented for all sensor nodes in $H[t]$. This operation dynamically adjusts the shape of the variant-egg forwarding zone, $F_{VE}[t+1]$, from time t to $t+1$.

The detailed operations of the variant-egg estimation and distributed VE-mobicast phases are described as follows.

4.1 Phase I: Egg estimation

All sensor nodes in $H[t]$ estimate the size and shape of variant-egg $F_{VE}[t+1]$ at time t for the upcoming forwarding zone, $Z[t+1]$. The shape of the variant-egg is calculated from the *Cassini oval*

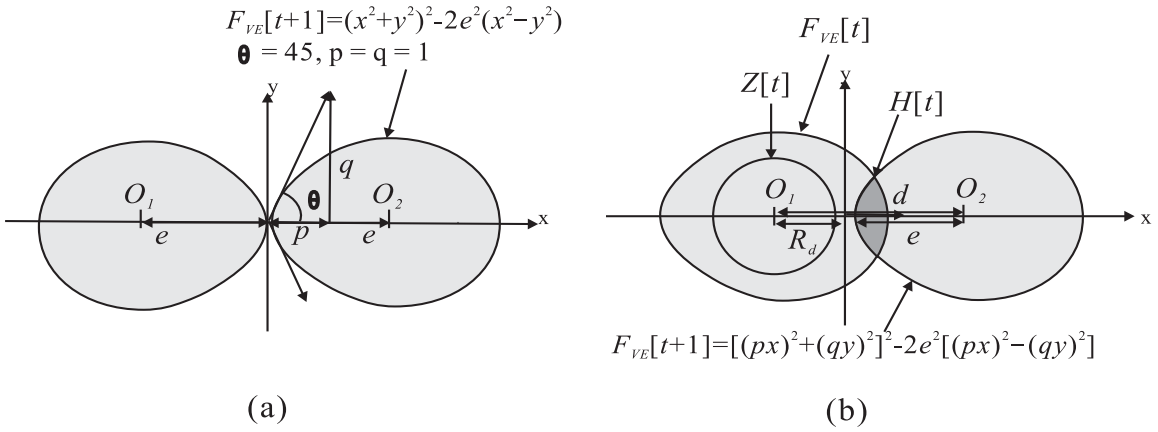

Figure 6: Equations of (a) the VE-mobicast and (b) the *Cassini oval*.

equation [29]. Based on the Cassini oval equation [29], the equation of our variant-egg forwarding zone is,

$$[(px)^2+(qy)^2]^2-2e^2[(px)^2-(qy)^2]=0, \text{ where } \tan\theta = q/p \text{ and } p\times q=1.$$

Observe that the forwarding zone can dynamically change shape by changing the ratio of p and q if the egg area is fixed, and px is p multiples of x and qy is q multiples of y, where $p\times q=1$. For instance with a fixed egg area, $p=q=1$, or $p=3$ and $q=\frac{1}{3}$. In our study, the area of our variant-egg forwarding zone $F_{VE}[t+1]$ is e^2, where $\theta=45^\circ$, $p=q=1$, and $e=\pi^{\frac{1}{2}}R_d$. The equation becomes

$$(x^2+y^2)^2-2e^2(x^2-y^2)=0.$$

Figure 6(a) shows an example of $F_{VE}[t+1]$ where O_1 and O_2 denote two fixed points, O_2 is the center of the variant-egg forwarding zone, and $2e$ is the distance between the fixed points, O_1 and O_2. In the following, our VE-mobicast routing protocol adopts half of the lemniscate as our variant-egg forwarding zone $F_{VE}[t+1]$. An example is shown in figure 6(b). The size and area of the forwarding zone are mainly decided by the value of e and are relative of R_d, which is the radius of delivery zone $Z[t]$. The distance, d, between $F_{VE}[t+1]$ and $Z[t]$ is $v*\Delta t$. Figure 7 shows an example of the variation in p and q. Figure 7(a) is a normal size and shape. Figure 7(b) shows the variant-egg forwarding zone if p is large and q is small. Figure 7(c) illustrates the variant-egg forwarding zone if p is small and q is large. In this paper, we only consider the case of $p=q=1$. To

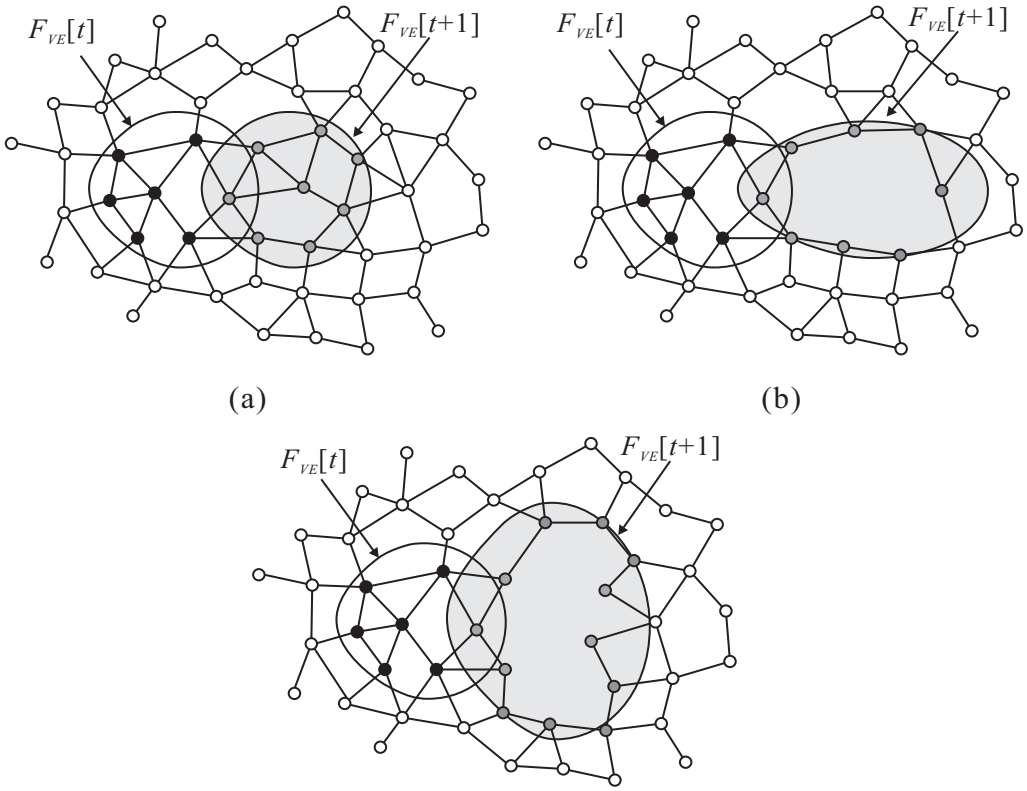

Figure 7: Dynamic sizes and shapes of $F_{VE}[t+1]$.

determine the "right" Cassini oval parameter, we discuss the initial estimated shape of the variable-egg in the simulation by choosing various values of p and q, where $p \times q = 1$. One important aspect is deciding whether or not sensor node (a,b) is located in variant-egg forwarding zone $F_{VE}[t+1]$. If $(x^2+y^2)^2 - 2e^2(x^2-y^2) = (a^2+b^2)^2 - 2e^2(a^2-b^2) \leq 0$, then (a,b) is located in variant-egg forwarding zone $F_{VE}[t+1]$. If $(x^2+y^2)^2 - 2e^2(x^2-y^2) = (a^2+b^2)^2 - 2e^2(a^2-b^2) > 0$, then (a,b) is out of variant-egg forwarding zone $F_{VE}[t+1]$. The egg estimation algorithm is given here.

S1: The first task is to decide whether or not sensor node P_1 at (a_1,b_1) is located in hold-and-forward zone $H[t] = F_{VE}[t] \cap F_{VE}[t+1]$. Sensor node P_1 is within $H[t]$ if P_1 is within $F_{VE}[t]$ and P_1 is also within $F_{VE}[t+1]$; that is, if $F_{VE}[t]$ is $(x_t^2+y_t^2)^2 - 2e_t^2(x_t^2-y_t^2) = 0$ and $F_{VE}[t+1]$ is $(x_{t+1}^2+y_{t+1}^2)^2 - 2e_{t+1}^2(x_{t+1}^2-y_{t+1}^2) = 0$, then $(x_t^2+y_t^2)^2 - 2e_t^2(x_t^2-y_t^2) = (a_1^2+b_1^2)^2 - 2e_t^2(a_1^2-b_1^2) \leq 0$ and $(x_{t+1}^2+y_{t+1}^2)^2 - 2e_{t+1}^2(x_{t+1}^2-y_{t+1}^2) = (a_1^2+b_1^2)^2 - 2e_{t+1}^2(a_1^2-b_1^2) \leq 0$. Figure 8(a) shows an example of P_1 located in $H[t] = F_{VE}[t] \cap F_{VE}[t+1]$.

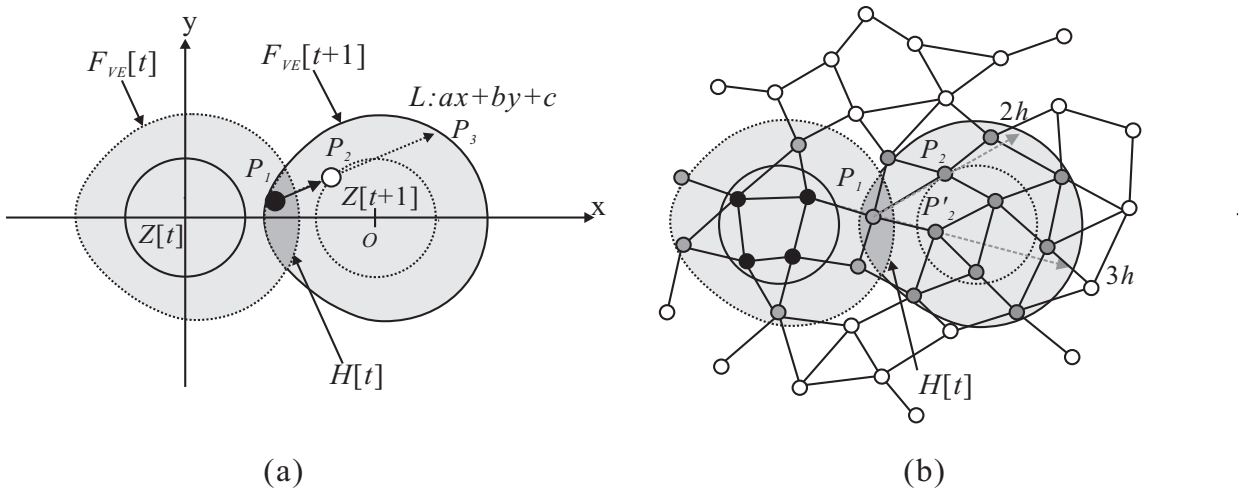

Figure 8: Estimation phase of a VE-mobicast.

S2: Let sensor node P_1 at (a_1, b_1) be within hold-and-forward zone $H[t]$, sensor node P_2 at (a_2, b_2) be within $F_{VE}[t+1]$, and P_1 and P_2 be a pair of neighboring nodes. A hop count is needed to estimate the hop-distance from P_1 through P_2 to the boundary of $F_{VE}[t+1]$. This hop count is very useful in phase II to provide a distributed algorithm of the variant-egg-based mobicast. Let the line equation of P_1 and P_2 be $ax+by+c=0$ and the equation of $F_{VE}[t+1]$ be $(x^2+y^2)^2-2e^2(x^2-y^2)$. Let P_3 be the intersection point of the line and $F_{VE}[t+1]$; that is, $ax+by+c=(x^2+y^2)^2-2e^2(x^2-y^2)$. Then, $\left|\overline{P_2P_3}\right|$is the distance between P_2 and P_3. Sensor node P_1, in anticipation, forwards a mobicast message through P_2 within $\frac{\left|\overline{P_2P_3}\right|}{r}+1$ hops, where r is the communication radius of the sensor node. An example is illustrated in figure 8(b), where the estimated hop counts from P_1 through P_2 and P'_2 are two and three, respectively.

4.2 Phase II: Distributed variant-egg-based mobicast

Phase I roughly estimates the initial size and shape of variant-egg-based forwarding zone, $F_{VE}[t+1]$ as illustrated in figure 7(a). In phase II, a distributed algorithm is developed to dynamically adjust the size and shape of variant-egg-based forwarding zone $F_{VE}[t+1]$ depending on the sensornet density, as illustrated in figure 7(b) and figure 7(c). Based on the estimated $F_{VE}[t+1]$ in phase I, a distributed algorithm of the VE-mobicast operation is presented for all sensor nodes in $H[t]$. This distributed

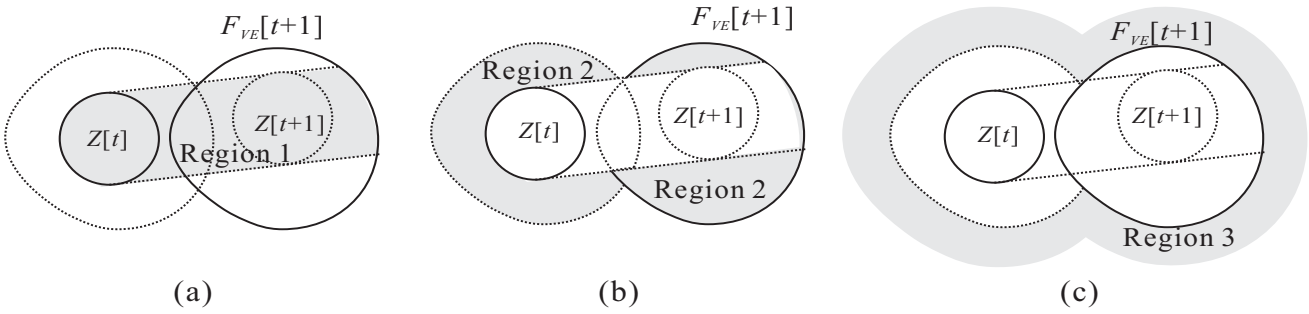

Figure 9: Three different regions.

operation dynamically adjusts the size and shape of $F_{VE}[t+1]$ from time t to time $t+1$.

A simple control packet, denoted $P_{VE}(p,q,\frac{h}{H},N_{11}N_{12}...N_{1i})_{t_x}$, is adopted in this paper for developing the distributed algorithm, where p and q are used to denote the initial shape of the forwarding zone, $\frac{h}{H}$ is used to limit the number of packets forwarded, $N_{11}N_{12}...N_{1i}$ maintain the path history, and packet P_{VE} is forwarded at time t_x. Assume that all sensor nodes are uniformly distributed in an area, and this area is divided into three kinds of region. Without loss of generality, we only consider the case of a pair of adjacent delivery zones, $Z[t]$ and $Z[t+1]$, and a pair of forwarding zones, $F_{VE}[t]$ and $F_{VE}[t+1]$, to explain these three regions as follows.

- Region 1: A path moves from $Z[t]$ to $Z[t+1]$, as illustrated in figure 9(a).
- Region 2: $F_{VE}[t]\cup F_{VE}[t+1]-$ Region 1, as illustrated in figure 9(b).
- Region 3: $\sim(F_{VE}[t]\cup F_{VE}[t+1])$, as illustrated in figure 9(c).

The distributed algorithm of the VE-mobicast operation is given here.

S1: A sensor node, P_i, is in $H[t]$ and P_j is in $F_{VE}[t+1]$, where P_i and P_j are neighboring nodes. Sensor node P_i initiates and floods a $P_{VE}(p,q,\frac{1}{H},P_i)_{t_x}$ packet to neighboring sensor node P_j at time $t_x=t_1$, where H is the estimated hop count calculated from phase I.

S2: Sensor node P_α receives the first packet, $P_{VE}(p,q,\frac{h_1}{H_1},N_{1,1}N_{1,2}...N_{1,i-1})_{t'_{x_1}}$, from N_{1i-1}, at time t'_{x_1}. Sensor node P_α waits for a period of time in order to receive at most $d-1$ different P_{VE} packets from $d-1$ neighboring nodes. Assuming that $P_{VE}(p,q,\frac{h_1}{H_1},N_{1,1}N_{1,2}\ldots N_{1,i-1})_{t'_{x_1}}$,

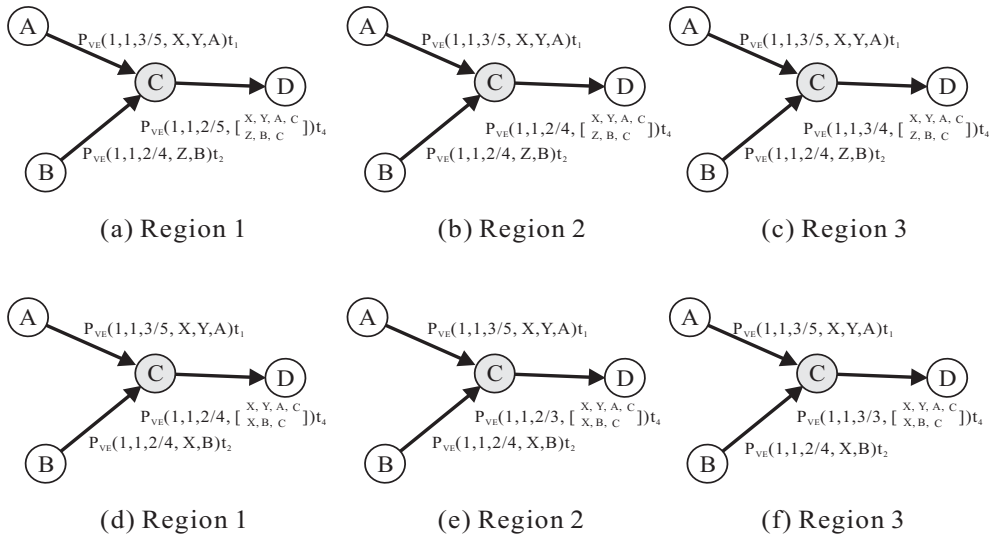

(a) Region 1 (b) Region 2 (c) Region 3

(d) Region 1 (e) Region 2 (f) Region 3

Figure 10: Examples of merging operations.

$P_{VE}(p,q,\frac{h_2}{H_2},N_{2,1}N_{2,2}...N_{2,i-1})_{t'_{x_2}}$, $\cdots$, and $P_{VE}(p,q,\frac{h_m}{H_m},N_{m,1}N_{m,2}\ ...\ N_{m,i-1}\ )_{t'_{xm}}$ packets are received at node P_α before time t'_y, then m P_{VE} packets are merged into one P_{VE} packet, denoted $P_{VE}(p,q,\frac{h_{merge}}{H_{merge}},\begin{bmatrix} N_{1,1}N_{1,2}...N_{1,i-1},P_\alpha \\ \vdots \\ N_{m,1}N_{m,2}...N_{m,i-1},P_\alpha \end{bmatrix})_{t'_y}$, where $m \le d-1$ and $t'_y = t'_{x_1} + d + backoff\_time$ and d is the degree of P_α. The merging operation, which is dependent on the position of sensor node P_α, is given here.

1. Let $\frac{h_{merge}}{H_{merge}} = \frac{\underset{1\le i\le m}{Min}\ h_i}{\underset{1\le i\le m}{Max}\ H_i}$ if P_α is in region 1.
2. Let $\frac{h_{merge}}{H_{merge}} = \frac{\underset{1\le i\le m}{Min}\ h_i}{\underset{1\le i\le m}{Min}\ H_i}$ if P_α is in region 2.
3. Let $\frac{h_{merge}}{H_{merge}} = \frac{\underset{1\le i\le m}{Max}\ h_i}{\underset{1\le i\le m}{Min}\ H_i}$ if P_α is in region 3.

S3: If there are the same n predecessor nodes for all path-histories of $\begin{bmatrix} N_{1,1}N_{1,2}...N_{1,i-1},P_\alpha \\ \vdots \\ N_{m,1}N_{m,2}...N_{m,i-1},P_\alpha \end{bmatrix}$, then let $H_{merge} = H_{merge} - n$. After that, the $P_{VE}(p,q,\frac{h_{merge}}{H_{merge}},\begin{bmatrix} N_{1,1}N_{1,2}...N_{1,i-1},P_\alpha \\ \vdots \\ N_{m,1}N_{m,2}...N_{m,i-1},P_\alpha \end{bmatrix})_{t'_y}$ packet is sent out and forwarded at time t'_y only if $\frac{h_{merge}}{H_{merge}} < 1$, where $t'_y = t'_{x_1} + d + backoff\_time$ and d is the degree of P_α.

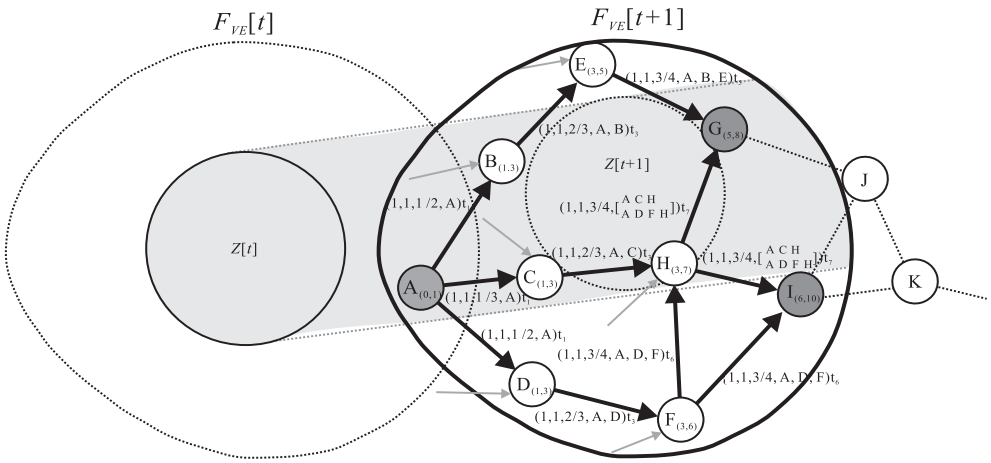

Figure 11: Scenario of the no "hole" problem.

Examples of merging operations in step **S2** are given in figure 10(a), where $p = q = 1$. If sensor node C is in region 1, sensor node C receives $P_{VE}(1,1,\frac{3}{5},X,Y,A)_{t_1}$ and $P_{VE}(1,1,\frac{2}{4},Z,B)_{t_2}$, and the merged packet is $P_{VE}(1,1,\frac{2}{5},\left[\begin{array}{c} X,Y,A,C \\ Z,B,C \end{array}\right])_{t_4}$ since the same predecessor sensor node does not exist. Figure 10(d) gives an explanation if sensor node C is in region 1, sensor node C receives $P_{VE}(1,1,\frac{3}{5},X,Y,A)_{t_1}$ and $P_{VE}(1,1,\frac{2}{4},X,B)_{t_2}$, and the merged packet is $P_{VE}(1,1,\frac{2}{4},\left[\begin{array}{c} X,Y,A,C \\ X,B,C \end{array}\right])_{t_4}$ because X is the same predecessor sensor node. As illustrated in figure 10(b), if sensor node C is in region 2 and sensor node C receives $P_{VE}(1,1,\frac{3}{5},X,Y,A)_{t_1}$ and $P_{VE}(1,1,\frac{2}{4},Z,B)_{t_2}$, then the merged packet is $P_{VE}(1,1,\frac{2}{4},\left[\begin{array}{c} X,Y,A,C \\ Z,B,C \end{array}\right])_{t_4}$, since the same predecessor sensor node does not exist. Figure 10(e) shows that if sensor node C is in region 2 and sensor node C receives $P_{VE}(1,1,\frac{3}{5},X,Y,A)_{t_1}$ and $P_{VE}(1,1,\frac{2}{4},X,B)_{t_2}$, then the merged packet is $P_{VE}(1,1,\frac{2}{3},\left[\begin{array}{c} X,Y,A,C \\ X,B,C \end{array}\right])_{t_4}$, since X is the same predecessor sensor node. Finally, as shown in figure 10(c), if sensor node C is in region 3 and sensor node C receives $P_{VE}(1,1,\frac{3}{5},X,Y,A)_{t_1}$ and $P_{VE}(1,1,\frac{2}{4},Z,B)_{t_2}$, then the merged packet is $P_{VE}(1,1,\frac{3}{4},\left[\begin{array}{c} X,Y,A,C \\ Z,B,C \end{array}\right])_{t_4}$, since the same predecessor sensor node does not exist. Figure 10(f) shows that if sensor node C is in region 3, sensor node C receives $P_{VE}(1,1,\frac{3}{5},X,Y,A)_{t_1}$ and $P_{VE}(1,1,\frac{2}{4},X,B)_{t_2}$, then the merged packet is $P_{VE}(1,1,\frac{3}{3},\left[\begin{array}{c} X,Y,A,C \\ X,B,C \end{array}\right])_{t_4}$, since X is the same predecessor sensor node.

In step **S3**, it was observed that $\frac{h_{merge}}{H_{merge}}$ is used to determine whether or not the P_{VE} packet should be forwarded, where h_{merge} denotes the hop number which the current P_{VE} packet traverses and H_{merge} is the estimated hop count toward the boundary of $F_{VE}[t+1]$. If the ratio of $\frac{h_{merge}}{H_{merge}} < 1$, the

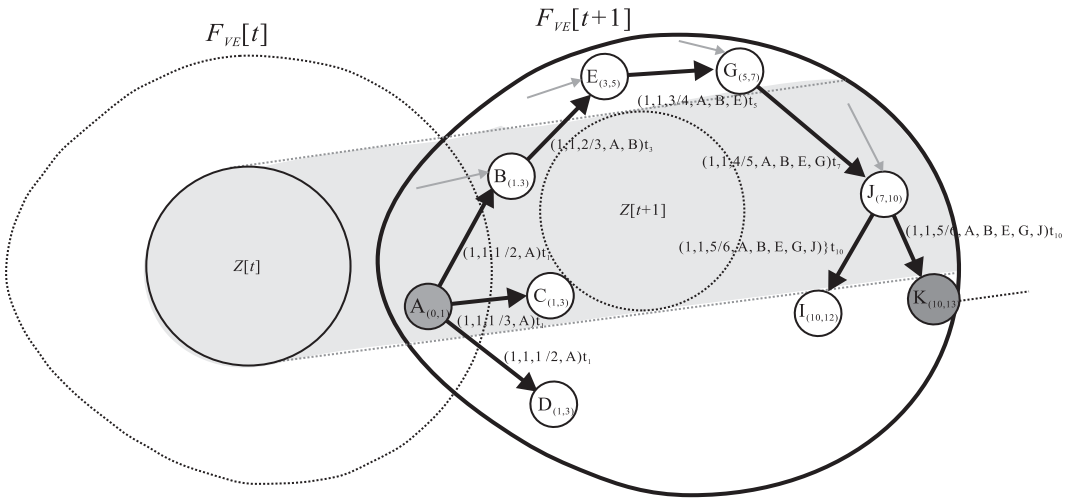

Figure 12: Scenario of the ”hole” problem.

P_{VE} packet is forwarded since $h_{merge} < H_{merge}$. If the ratio of $\frac{h_{merge}}{H_{merge}} \geq 1$, the P_{VE} packet is not forwarded since $h_{merge} \geq H_{merge}$.

Finally, two scenarios are given in figures 11 and 12 to discuss the effect of the ’hole’ problem. Let $N_{(\alpha,\beta)}$ denote a sensor node, N, which receives its first P_{VE} message at time t_α and forwards the merged P_{VE} message at time t_β. Observe that the initial estimated shapes of the variable-egg in phase I (egg estimation phase) for the two cases are the same. It is shown in figures 11 and 12 that node $B_{(1,3)}$ has the same estimated $H = 2$, but the P_{VE} message is stopped at node $G_{(5,8)}$ in figure 11 and is stopped at node $K_{(10,13)}$ in figure 12. This is because figure 11 has no ’hole’ in $F_{VE}[t+1]$, but figure 12 has a ’hole’ in $F_{VE}[t+1]$. In these two cases, the final shapes of these two forwarding zones $F_{VE}[t+1]$, greatly differ, due to the dynamic adjustment capability of the VE-mobicast routing protocol.

5 Performance analysis

We provide theoretically proven bounds for the predictive accuracy and energy efficiency of our algorithm, and perform an analysis of our algorithm in terms of the number of messages used and running time. The simulation results are then analyzed.

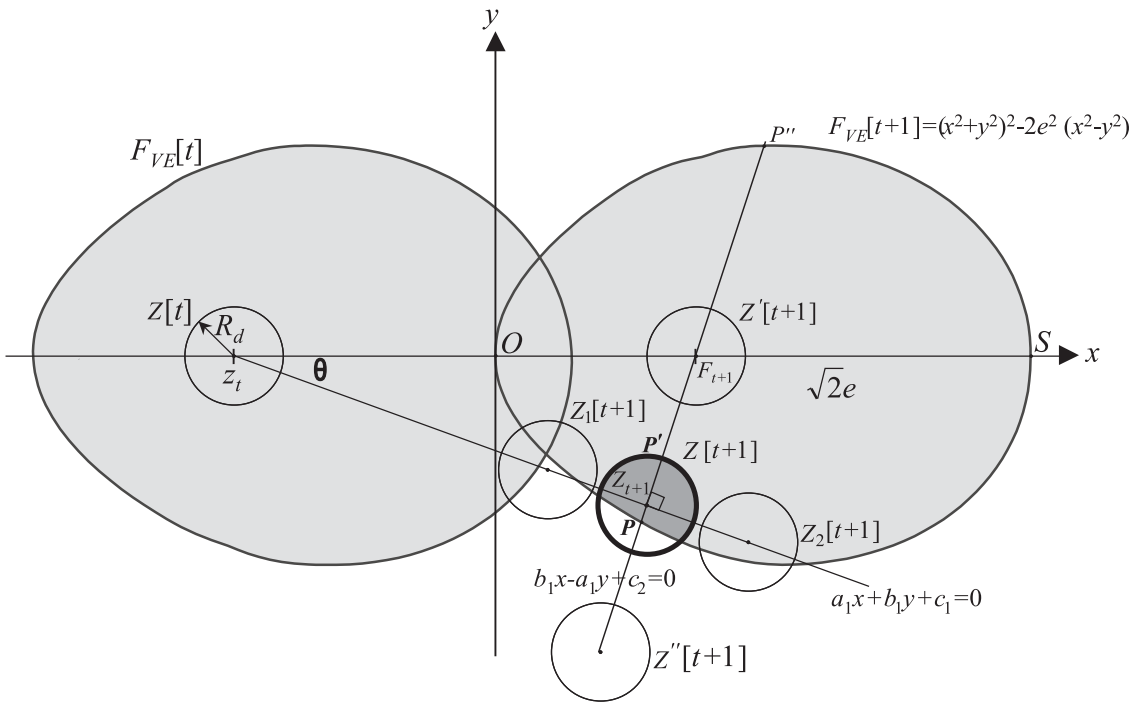

Figure 13: Example for the mathematical analysis.

5.1 Mathematical analysis

All sensor nodes are assumed in the analysis to be randomly and uniformly deployed in the network. We also assume that the numbers of sensor nodes in a $Z[t+1]$ and $F_{VE}[t+1]$ are approximately represented by the coverage area of $Z[t+1]$ and $F_{VE}[t+1]$ divided by the transmission area of a sensor node, respectively. The predictive accuracy is defined as the percentage of sensor nodes located in both $Z[t+1]$ and $F_{VE}[t+1]$ divided by the total number of sensor nodes in $Z[t+1]$. We have the following results.

Lemma 1 *The low bound of the predictive accuracy, denoted as* RA_{low_bound}*, is* $\frac{2\int_{R_d-|\overline{PP'}|}^{R_d}\sqrt{{R_d}^2-x^2}dx}{\pi {R_d}^2}$*, for* $0<|\overline{PP'}|=R_d-(|\overline{F_{t+1}Z_{t+1}}|-|\overline{F_{t+1}P}|)<2R_d$*, where P is the intersection point of line* $b_1x-a_1y+c_2=0$ *and* $F_{VE}[t+1]$*,* P' *is the intersection point of line* $b_1x-a_1y+c_2=0$ *with* $Z[t+1]$*,* R_d *is the radius of the delivery zone* $Z[t]$*,* F_{t+1} *is the focus of* $F_{VE}[t+1]$*, and* Z_{t+1} *is the point closest to* F_{t+1}*.*

Proof. In our analysis, RA_{low_bound} is estimated by the overlapping ratio of $Z[t+1]$ with $F_{VE}[t+1]$. Assume that Z_t is the center of $Z[t]$, Z_{t+1} is the center of $Z[t+1]$, and F_{t+1} is the focus of $F_{VE}[t+1]$. Let Z_{t+1} be the point closest to F_{t+1}, such that $\overline{Z_{t+1}F_{t+1}}$ is minimal. A line equation $a_1x+b_1y+c_1=0$ is determined by going through Z_t and Z_{t+1}. The path along line $a_1x+b_1y+c_1=0$ is the moving path from $Z[t]$ to $Z[t+1]$ with rotation angle θ. Observe that $Z[t+1]$ has a maximal overlapping area with $F_{VE}[t+1]$, since Z_{t+1} is closest to F_{t+1}. As illustrated in figure 13, $Z_1[t+1]$ and $Z_2[t+1]$ are not adopted, because $Z[t+1]$ along line $a_1x+b_1y+c_1=0$ is closest to F_{t+1}. The RA_{low_bound} is calculated as follows. A vertical line, which passes through both F_{t+1} and Z_{t+1}, is $b_1x-a_1y+c_2=0$, where the slope of the vertical line is $\frac{b_1}{a_1}$. Observe that Z_{t+1} is the intersection point of $a_1x+b_1y+c_1=0$ and $b_1x-a_1y+c_2=0$; i.e., $a_1x+b_1y+c_1=b_1x-a_1y+c_2=0$. In addition, P is the intersection point of $b_1x-a_1y+c_2=0$ and $F_{VE}[t+1]$; i.e., $b_1x-a_1y+c_2=(x^2+y^2)^2-2e^2(x^2-y^2)=0$. Denote $\left|\overline{F_{t+1}Z_{t+1}}\right|$ as the distance from F_{t+1} to Z_{t+1} and $\left|\overline{F_{t+1}P}\right|$ as the distance from F_{t+1} to P. Let P' be the intersection point of line $b_1x-a_1y+c_2=0$ with $Z[t+1]$ as shown in figure 13, and $\left|\overline{PP'}\right|=R_d-(\left|\overline{F_{t+1}Z_{t+1}}\right|-\left|\overline{F_{t+1}P}\right|)$. The low bound of the predictive accuracy is calculated as follows.

$$RA_{low\_bound}=\begin{cases}0, & \text{for } \left|\overline{PP'}\right|<0,\\ \frac{\text{area of } Z[t+1]\cap\text{area of } F_{VE}[t+1]}{\text{area of } Z_{VE}[t+1]}=\frac{2\int_{R_d-\left|\overline{PP'}\right|}^{R_d}\sqrt{{R_d}^2-x^2}dx}{\pi{R_d}^2}, & \text{for } 0\le\left|\overline{PP'}\right|\le 2R_d,\\ 1, & \text{for } 2R_d<\left|\overline{PP'}\right|.\end{cases}$$ ■

An example is given in figure 13: RA_{low_bound} of $Z'[t+1]$ is 100%, where $2R_d<\left|\overline{PP'}\right|$; RA_{low_bound} of $Z''[t+1]$ is 0%, where $\left|\overline{PP'}\right|<0$; and RA_{low_bound} of $Z[t+1]$ is $\frac{2\int_{R_d-\left|\overline{PP'}\right|}^{R_d}\sqrt{{R_d}^2-x^2}dx}{\pi{R_d}^2}$, where $0\le\left|\overline{PP'}\right|\le 2R_d$. The low bound of energy consumption of the VE-mobicast protocol can thus be investigated.

Lemma 2 *The low bound of energy consumption of the VE-mobicast protocol from time t to $t+1$ is $N_{total}\times(P_t+(d-1)P_r+P_{switch})$, where N_{total} is the total number of sensor nodes in $F_{VE}[t+1]$, d is the average degree of all sensor nodes, P_t is the power consumption cost of one data transmission operation, P_r is the power consumption cost of one data reception operation, and P_{switch} is the power consumption cost of a switching operation to switch a sensor node from the sleep mode to the active*

mode.

Proof. The low bound of energy consumption is calculated by performing the mobicast message forwarding operation to wake up all sensor nodes in $F_{VE}[t+1]$. Each mobicast message forwarding operation for each sensor node consumes at least as much power as $P_t + (d-1) \times P_r + P_{switch}$, where d is the average degree of sensor nodes of $F_{VE}[t+1]$. All sensor nodes are assumed to be uniformly deployed, and the total number of sensor nodes in $F_{VE}[t+1]$ can be decided as follows. As illustrated in figure 13, denote S as the intersection point of the linear equation $y=0$ and $F_{VE}[t+1]$; i.e., $x^4 - 2e^2x^2 = 0$. Then the coordinate of S is $(\sqrt{2}e, 0)$, where $\left|\overline{OS}\right|$ is $\sqrt{2}e$. Let F_{Area} denote the area of $F_{VE}[t+1]$, where $F_{Area} = \int_0^{\sqrt{2}e}(x^2+y^2)^2 - 2e^2(x^2-y^2)dxdy$. The total number of sensor nodes in $F_{VE}[t+1]$ is approximately equal to $N_{total} = \frac{F_{Area}}{Rt^2} = \frac{\int_0^{\sqrt{2}e}(x^2+y^2)^2-2e^2(x^2-y^2)dxdy}{Rt^2}$, where R_t is the transmission radius of each sensor node. Let d_{P_α} denote the degree of sensor node P_α in $F_{VE}[t+1]$, and the low bound of energy consumption is

$$\sum_{\alpha=1}^{N_{total}} (P_t + (d_{P_\alpha} - 1)P_r + P_{switch}) \approx N_{total} \times (P_t + (d-1)P_r + P_{switch}). \blacksquare$$

In addition, we perform an analysis of our algorithm in terms of the number of messages used and the running time.

Lemma 3 *The total number of mobicast messages of the VE-mobicast protocol from time t to $t+1$ is $N_{total} \times (d-1)$, where N_{total} is the total number of sensor nodes in $F_{VE}[t+1]$ and d is the average degree of all sensor nodes.*

Proof. The approximate total number of mobicast messages is obtained by calculating the total number of mobicast messages in $F_{VE}[t+1]$. On average, every sensor node receives at least $d-1$ mobicast messages from $d-1$ neighboring nodes, where d is the average degree of all sensor nodes. Given that d_{P_α} is the degree of sensor node P_α in $F_{VE}[t+1]$ and $N_{total} = \frac{F_{Area}}{Rt^2} = \frac{\int_0^{\sqrt{2}e}(x^2+y^2)^2-2e^2(x^2-y^2)dxdy}{Rt^2}$, the total number of mobicast messages in the $F_{VE}[t+1]$ is

$$\sum_{\alpha=1}^{N_{total}} (d_{P_\alpha} - 1) \approx N_{total} \times (d-1). \blacksquare$$

Lemma 4 *The running time of the VE-mobicast protocol from time t to $t+1$ is $(\frac{\sqrt{2}e}{R_t}-1)\times((d-1)T_r+T_b)$, where $\frac{\sqrt{2}e}{R_t}$ is the diameter of the $F_{VE}[t+1]$, d is the average degree of all sensor nodes, T_r is the time cost of data transmission, and T_b is the random backoff time.*

Proof. The approximate running time is calculated by the longest path from a node in $H[t]$ to a border node in $F_{VE}[t+1]$. First, the hop number of the longest path is estimated as follows. As shown in figure 13, the distance of the longest path is $\left|\overline{OS}\right| = \sqrt{2}e$, and its hop number is $\frac{\sqrt{2}e}{R_t}$. If d_{P_α} is the degree of sensor node P_α in the $F_{VE}[t+1]$, then the running time of the VE-mobicast protocol is

$$\sum_{\alpha=1}^{\frac{\sqrt{2}e}{R_t}-1}(d_{P_\alpha}-1)T_r+T_b \approx (\frac{\sqrt{2}e}{R_t}-1)\times((d-1)T_r+T_b). \blacksquare$$

5.2 Simulation result

Our paper presents a variant-egg-based mobicast protocol. To evaluate our VE-mobicast protocol (VE-mobicast), Huang *et al.*'s mobicast protocol (mobicast) [10], and the FAR protocol (FAR) [12], all these protocols are mainly implemented using the NCTUns 2.0 simulator and emulator [28]. The system parameters are given below. To discuss the effect of the *network density* (ND) of a sensornet, our simulator considers nine different sensornet areas: 1000×400, 1000×500, 1000×600, 1000×700, 1000×800, 1000×900, 1000×1000, 1000×1100, and 1000×1200 m^2 with 800 randomly distributed sensor nodes. With the same number of sensor nodes, the ND is changed due to the different sensornet sizes. The communication radius of each sensor node is 35 m. Each sensor node knows its own location information. The velocity of the delivery zone is 40 m/s and its radius is 45 m. Assume that the consumption of power is denoted as *n* mW (milliWatts). With the same power assumption model in [7], the power consumption of the sleeping mode for a sensor node is 130 mW. The power consumption of the active mode of a sensor node is 830 mW. The power consumption of the transmission/reception mode of a sensor node is 1400 mW.

Before describing the performance metrics, the *rotation frequency* (RF) and *rotation angle* (RA) are defined. The RA is the angle between the two zones, $Z[t]$ and $Z[t+1]$, if rotation (or turn) occurs

at times t and $t+1$. The RA ranges from 5° to 50° in the simulation. The RF is the frequency of changing the rotation angle for a spatiotemporal application. The RF ranges from 10% to 100% in our simulation. The performance metrics to be observed are:

- The *predictive accuracy* (PA) is the percentage of sensor nodes located in both $Z[t+1]$ and $F_{VE}[t+1]$ (or $F[t+1]$) divided by the total number of sensor nodes in $Z[t+1]$, i.e., PA = 100% if all nodes in $Z[t+1]$ are located in $F_{VE}[t+1]$ (or $F[t+1]$).

- The *packet overhead ratio* (POR) is the total number of packets that all sensor nodes transmit, including the control and mobicast messages, divided by the minimum number of packets used in our VE-mobicast protocol.

- The *throughput* (TP) is the total number of data packets the mobile entity receives from sensor nodes in $Z[t+1]$ per second.

- The *power consumption ratio* (PCR) is the total power consumption of all sensor nodes divided by the minimum power consumption of our VE-mobicast protocol.

An efficient mobicast routing protocol in a sensornet is achieved with a high PA, low POR, high TP, and low PCR. Before discussing the simulation results, we initially discuss the initial shape of the variable-egg from various perspectives.

5.2.1 The initial estimated shape of the variable-egg

The initial estimated shape of the variable-egg in phase I (the egg-estimation phase) of the VE-mobicast routing protocol is mainly determined by the values of p and q, where $p \times q = 1$. With the same convergent area, figure 7(a)$\sim$(c) shows three different shapes of the variant-egg forwarding zone, where $p = q = 1$, $p = 3$ and $q = \frac{1}{3}$, and $p = \frac{1}{3}$ and $q = 3$, respectively. In our approach, the initial estimated shape of the variable-egg is not its final shape. Based on the initial estimated shape of the variable-egg, our approach offers a dynamic adjustment mechanism to provide a final shape variable-egg dependent on the actual network topology. The optimal shape of the forwarding zone can be accurately calculated if the global network topology is known in advance. Without the aid

of the global network topology information, our approach provides a nearly optimal shape for the forwarding zone. In this subsection, we investigate the effects on the predictive accuracy of choosing different values of p and q to determine the "right" Cassini oval parameter in the initial estimated variable-egg. A predictive accuracy gap is defined so that we can investigate the effects of PA for different values of p and q. The predictive accuracy gap is defined as $G_{PA}(p,q) = PA_{optimal} - PA_{p,q}$, where $PA_{p,q}$ denotes the predictive accuracy (PA) under given values of p and q, where $p \times q = 1$. In our simulation, we use (p,q) to denote one pair of possible values of p and q, where $p \times q = 1$. An optimal predictive accuracy $(PA_{optimal}) = 100\%$ indicates that all sensor nodes in $Z[t+1]$ are located in $F_{VE}[t+1]$. It is observed that the $PA_{p,q}$ is very close to the $PA_{optimal}$, while the $G_{PA}(p,q)$ is nearly zero. Given a (p,q), the shape of the initial estimated variable-egg is near the optimal forwarding zone if the $G_{PA}(p,q)$ is nearly zero.

To illustrate the influence of the $G_{PA}(p,q)$, various combinations of (p,q) were considered in order to observe the influences on the $G_{PA}(p,q)$ as follows. Figure 14(a) shows the initial simulation results of the average $G_{PA}(p,q)$ on the impact of various RAs (ranging from 5° to 50°). The average $G_{PA}(p,q)$ was calculated by setting $10\% \leq \text{RF} \leq 100\%$ and ND = 10 nodes/m^2. Figure 14(a) shows that the average $G_{PA}(p,q)$ ranges from 10 to 19.5, when $5^\circ \leq \text{RA} \leq 50^\circ$. This illustrates that the smaller the rotation angle is, the lower the $G_{PA}(p,q)$ will be. For each curve, it can be observed that the $G_{PA}(1,1) < G_{PA}(p',q)$ and $G_{PA}(1,1) < G_{PA}(p'',q)$, where $p' < 1$ and $p'' > 1$. This justifies $(1,1)$ being the best choice for (p,q) as the initial estimated variable-egg. Figure 14(b) shows the simulation results of the average $G_{PA}(p,q)$ on the impact of various RFs, where $10\% \leq \text{RF} \leq 100\%$. The average $G_{PA}(p,q)$ was calculated using the average value of the PA for all possible NDs (ranging from 6 to 20 nodes/m^2), with the RA fixed at 15°. Figure 14(b) shows that all average $G_{PA}(p,q)$ values ranged from 4 to 24, and the smaller the RF is, the lower the $G_{PA}(p,q)$ will be. For each curve, we observed the same result that the $G_{PA}(1,1) < G_{PA}(p',q)$ and $G_{PA}(1,1) < G_{PA}(p'',q)$, where $p' < 1$ and $p'' > 1$. We observed the same result that $(1,1)$ was the best selection of (p,q) as the initial estimated variable-egg. In addition, figure 14(c) illustrates the simulation results of the average $G_{PA}(p,q)$ on the impact of various NDs, where $6 \leq \text{ND} \leq 20$ nodes/m^2. The average

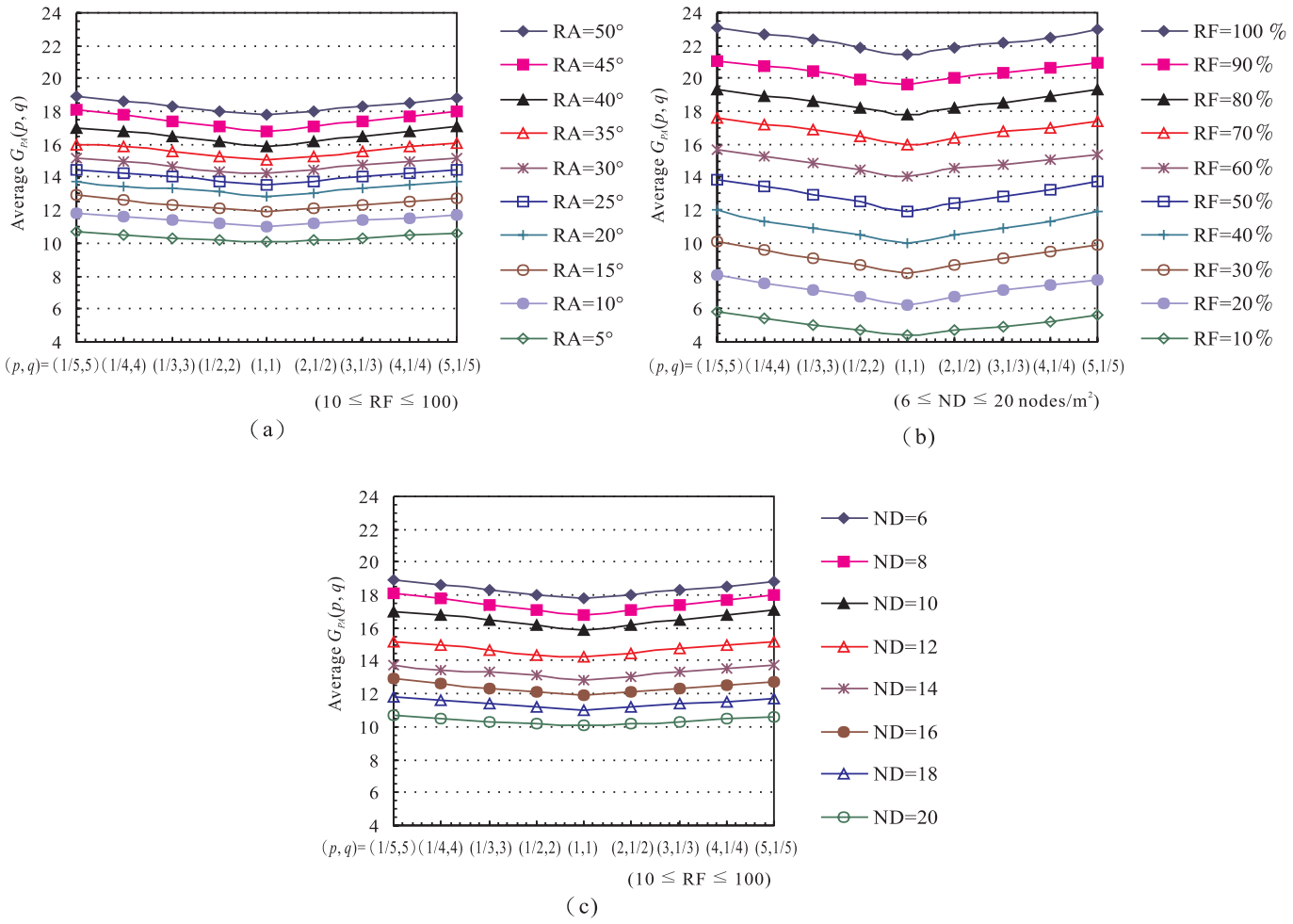

Figure 14: Performance of the average predictive accuracy gap $G_{PA}(p,q)$ vs. (a) the rotation angle ($10\% \leq \text{RF} \leq 100\%$), (b) the rotation frequency ($6 \leq \text{ND} \leq 20$ nodes/m^2), (c) the network density ($10\% \leq \text{RF} \leq 100\%$).

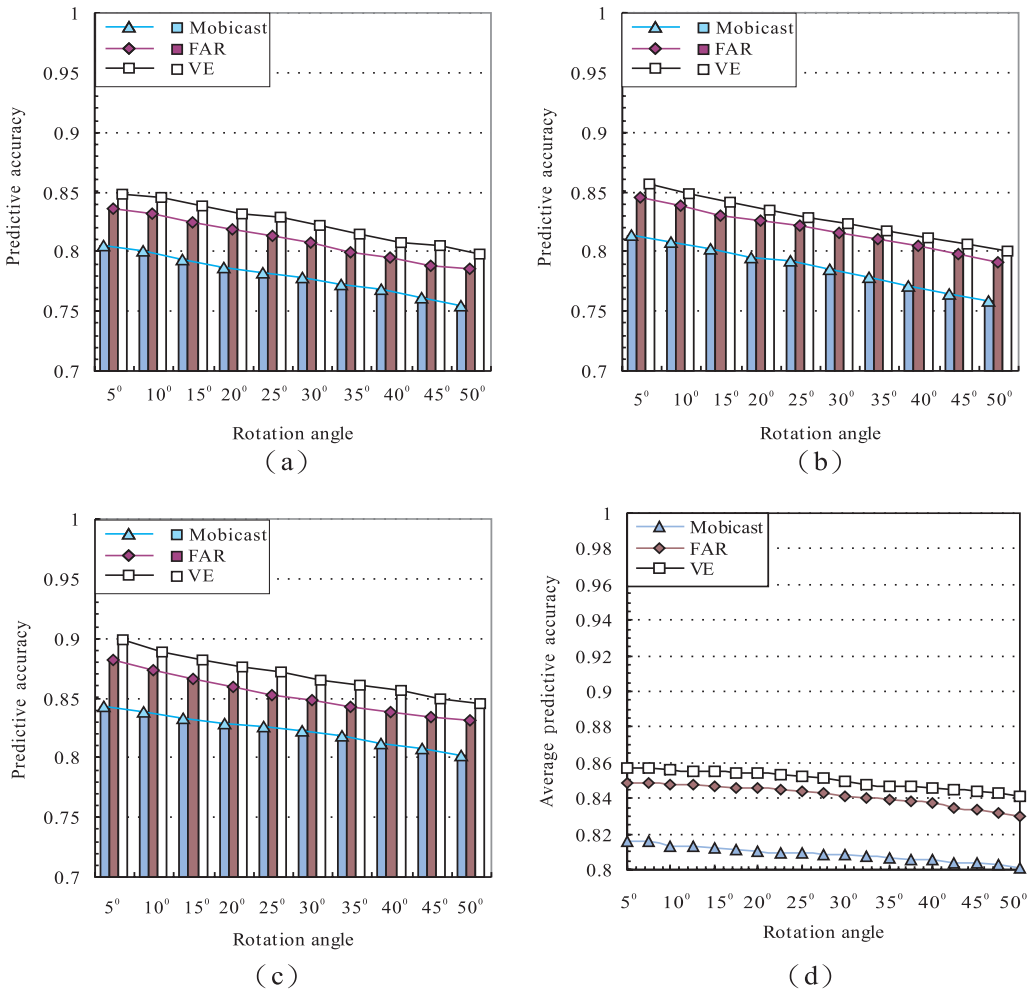

Figure 15: Performance of the predicitive accuracy vs. the rotation angle, where (a) the rotation frequency = 10%, (b) the rotation frequency = 50%, (c) the rotation frequency = 100%, and (d) 10% $\leq$ the rotation frequency $\leq$ 100%.

$G_{PA}(p,q)$ was calculated using the average value of the PAs for all possible RFs (ranging from 10% to 100%) with the RA fixed at 15°. Figure 14(c) shows that the smaller the ND is, the lower the $G_{PA}(p,q)$ will be, and all average $G_{PA}(p,q)$ values ranged from 10 to 20. We observed that $(1,1)$ was the best selection of (p,q) as illustrated in figure 14(c). Consequently, it is reasonable to choose (1, 1) as the "right" Cassini oval parameter in phase I (the egg-estimation phase) of the VE-mobicast routing protocol. In the following, we discuss the simulation results from various perspectives, where $(p,q) = (1,1)$.

5.2.2 Predictive accuracy (PA)

The simulation results of the PA under various RAs, RFs, and NDs are shown in figures 15, 16, and 17. Figure 15 shows the observed PA under various RFs and RAs, where the ND is fixed at 10 nodes/m^2. A mobicast routing protocol with the high predictive accuracy implies that the value of its PA was high. Figure 15(a)$\sim$(c) shows the performances of the mobicast, FAR, and VE-mobicast routing protocols in terms of the PA, under RFs of 10%, 50%, and 100%. The PA was low where the RF was high for various RAs. For each case, the curve of the PA of the mobicast was lower than that of the FAR, and the curve of the PA of the FAR was lower than that of the VE-mobicast. In addition, the lower the RA is, the higher the PA will be. Figure 15(d) shows the average PA results for the mobicast, FAR, and VE-mobicast. The average PA was calculated using the average value of the PA for all possible RFs (ranging from 10% to 100%). The average PA of the mobicast was $<$ that of the FAR which was $<$ that of the VE-mobicast from the perspective of RA. This is because the mobicast offers local compactness for deciding the forwarding zone. The mobicast and FAR do not offer a tolerance mechanism if a rotation (or a turn) occurs. In addition, the FAR had a better PA since the FAR is a reliable protocol. It was observed that when the RA was high, then the PA of the FAR slightly decreased. Our VE-mobicast provides an adaptive shape of the variant-egg to improve the PA for various RAs.

Figure 16 illustrates the performance of the PA under various RFs and NDs, with the RA fixed at 15°. Figure 16(a)$\sim$(c) shows the performances of the PA of the mobicast, FAR, and VE-mobicast routing protocols, under the NDs of 6, 12, and 20 nodes/m^2. In general, the PA drops as the ND decreases. For each case, the lower the RF is, the higher the PA will be. Figure 16(d) illustrates the average PA results for the mobicast, FAR, and VE-mobicast, where the average PA was calculated using the average value of the PA for all possible NDs (ranging from 6 to 20 nodes/m^2). We observed that the average PA of the mobicast $<$ that of the FAR $<$ that of the VE-mobicast from the perspective of RF. Figure 17 illustrates the performance of the PA under various NDs and RAs, with the RF fixed at 50%. Figure 17(a)$\sim$(c) shows the performances of the PA of the mobicast, FAR, and VE-mobicast routing protocols, under RAs of 5°, 30°, and 50°. We observed that the PA drops as the RA

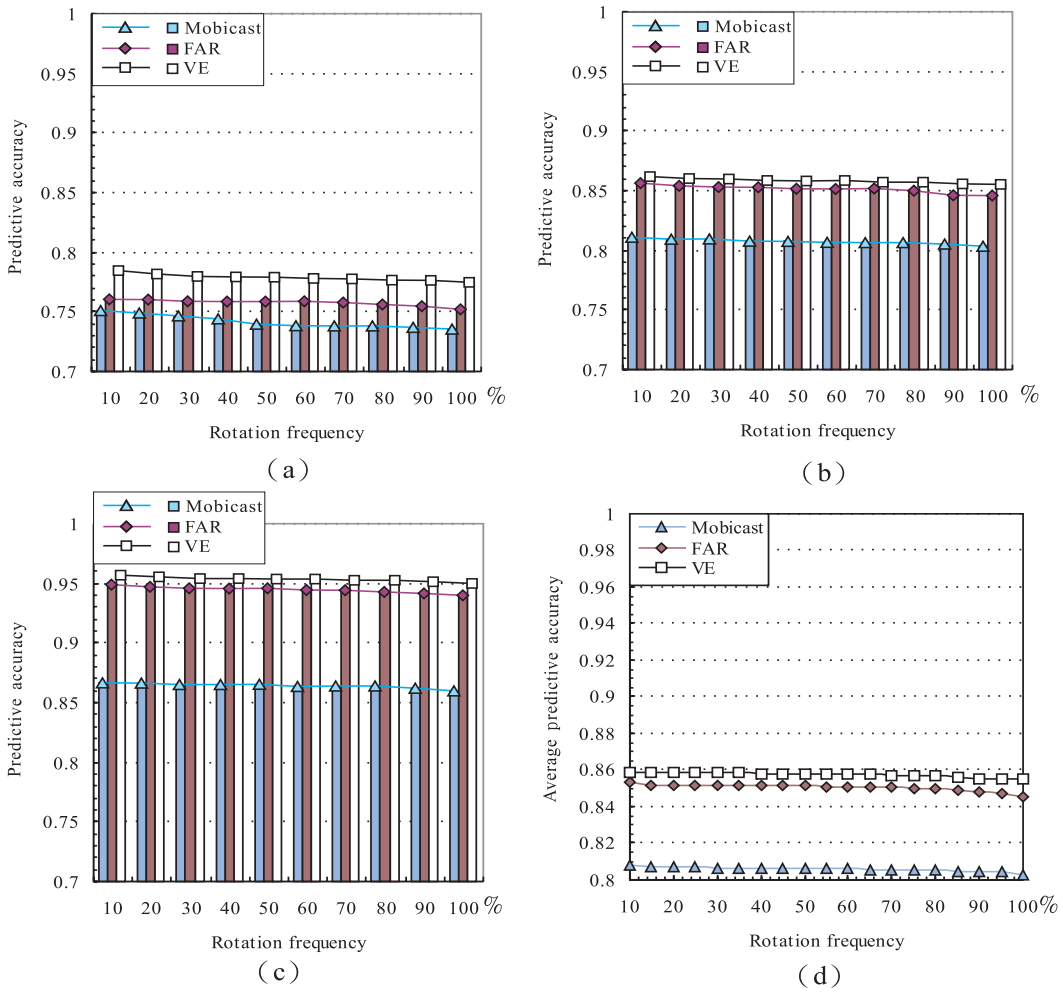

Figure 16: Performance of the predicitive accuracy vs. the rotation frequency, where (a) the network density = 6 nodes/m^2, (b) the network density = 12 nodes/m^2, (c) the network density = 20 nodes/m^2, and (d) 6 nodes/m^2 $\leq$ the network density $\leq$ 20 nodes/m^2.

increases. For each case, the higher the ND is, the higher the PA of the VE-mobicast will be. Figure 17(d) shows the average PA results for the mobicast, FAR, and VE-mobicast, where the average PA was calculated using the average value of the PA for all possible rotation angles (ranging from 5° to 50°). In conclusion, the average PA of the mobicast $<$ that of the FAR $<$ that of the VE-mobicast from the perspective of RA, RF, and ND.

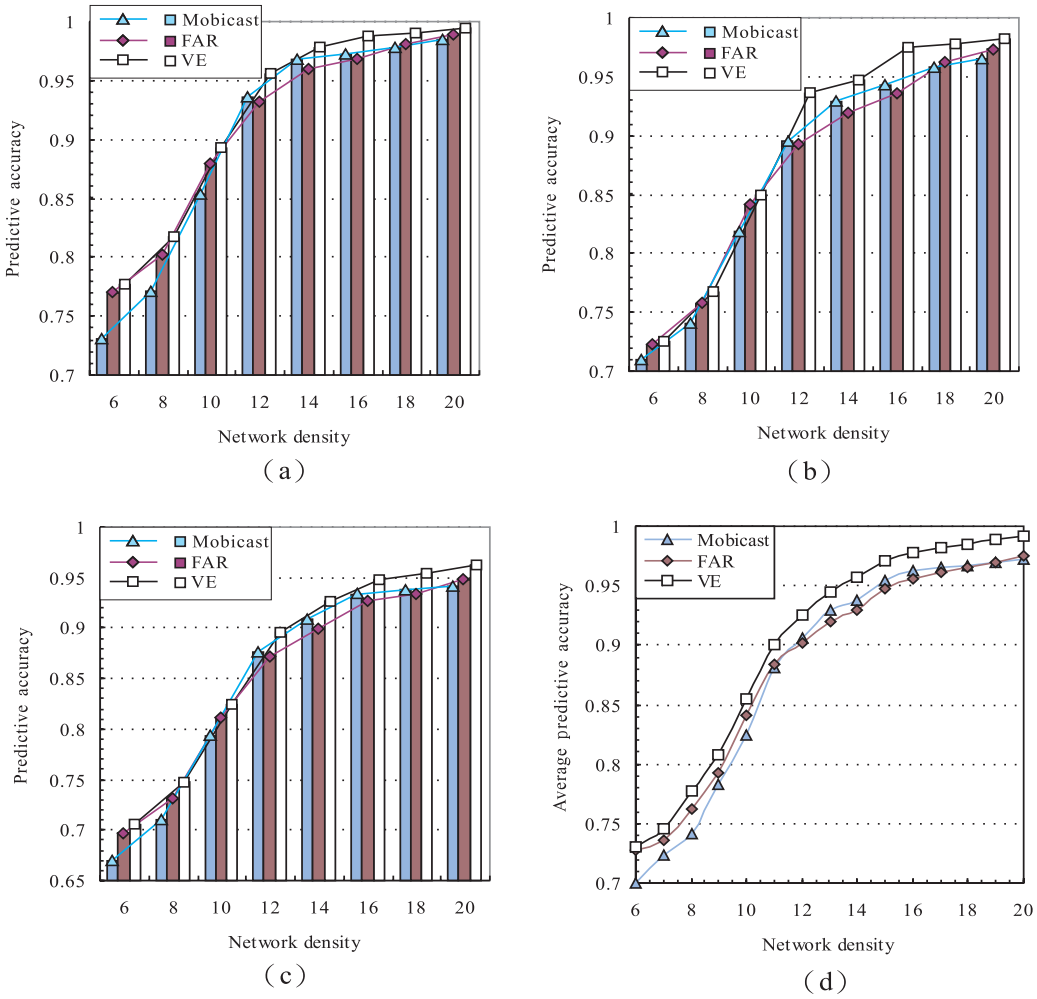

Figure 17: Performance of the predictive accuracy vs. the network density, when (a) the rotation angle = 5°, (b) the rotation angle = 30°, (c) the rotation angle = 50°, and (d) 5° ≤ the rotation angle ≤ 50°.

5.2.3 Packet overhead ratio (POR)

Figure 18 shows the simulation results of the packet overhead ratio (POR) for the VE-mobicast, mobicast, and FAR. The higher the value of POR is, the larger the number of packets will be. Figure 18(a) shows the performance of the average POR vs. various RAs (ranging from 5° to 50°), where 10% ≤ RF ≤ 100%, with the ND fixed at 10 nodes/m^2. Figure 18(b) shows the performance of the average POR vs. various RFs (ranging from 0% to 100%), where 6 ≤ ND ≤ 20 nodes/m^2, with the RA fixed at 15°. Figure 18(c) shows the performance of the average POR vs. various NDs (ranging from 6 to 20 nodes/m^2), where 5° ≤ RA ≤ 50°, with the RF fixed at 50%. For each case, we observed

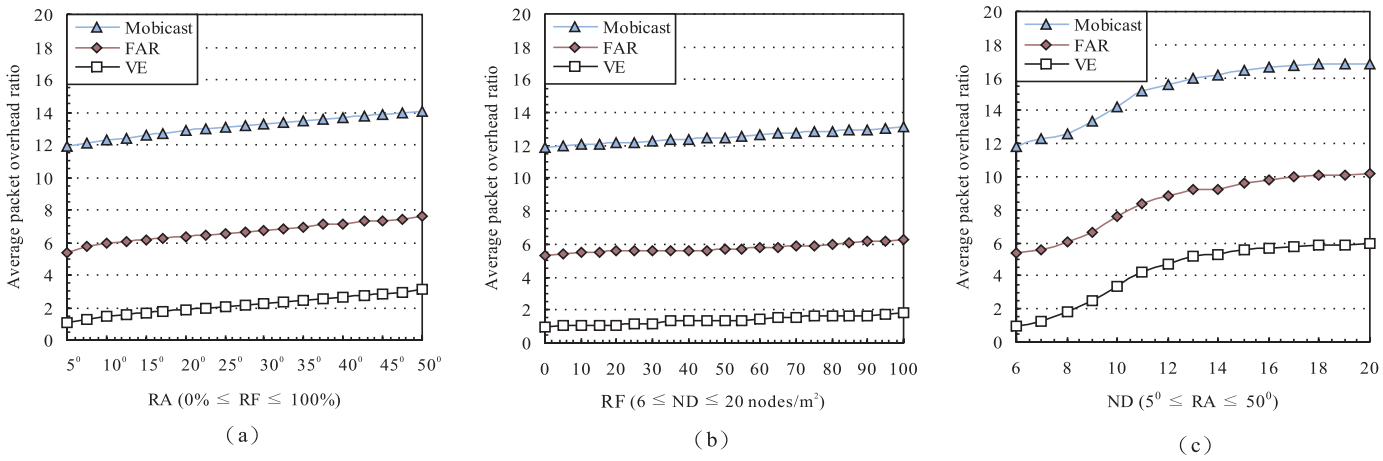

Figure 18: Performance of average packet overhead ratio (POR) vs. (a) rotation angle (RA), (b) rotation frequency (RF), and (c) network density (ND).

that the curve of the POR of the mobicast was higher than that of the FAR, and the curve of the POR of the FAR was also higher than that of the VE-mobicast. That is, the average POR of the mobicast $>$ that of the FAR $>$ that of the VE-mobicast. The mobicast protocol [11] always offered many packets to maintain the topological information by periodically broadcasting and exchanging the local compactness to decide the forwarding zone. When the local compactness was low, the mobicast routing protocol woke up additional sensor nodes to forward the mobicast message. The POR of the FAR was lower than that of the mobicast routing protocol. This is because the main cost of the POR of the FAR consists of the control packets during the neighborhood discovery protocol. After constructing the spatial neighborhood, the FAR requires fewer sensor nodes to transmit mobicast messages. Our distributed VE-mobicast used fewer control packets than the FAR.

5.2.4 Throughput (TP)

Figure 19 gives the simulation results of TP for the VE-mobicast, mobicast, and FAR. The higher the value of TP is, the higher the performance of the mobicast routing protocol will be. Figure 19(a) shows the performance of the average TP vs. various RAs (ranging from 5° to 50°), where 10% $\leq$ the RF $\leq$ 100%, with the ND fixed at 10 nodes/m^2. Figure 19(b) shows the performance of the average TP vs. various RFs (ranging from 0% to 100%), where 6 $\leq$ the ND $\leq$ 20 nodes/m^2, with the

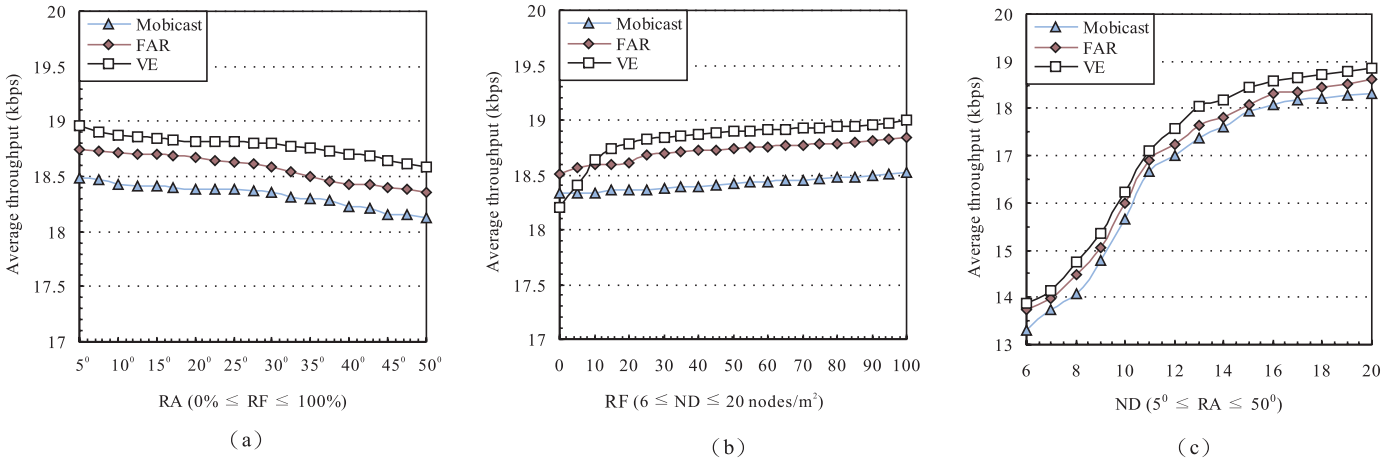

Figure 19: Performance of the average throughput (TP) vs. (a) rotation angle (RA), (b) rotation frequency (RF), and (c) network density (ND).

RA fixed at 15°. Figure 19(c) shows the performance of the average TP vs. various NDs (ranging from 6 to 20 nodes/m^2), where 5° $\leq$ the RA $\leq$ 50°and the RF is fixed to 50%. This is a case of the overhead being reduced at the expense of reducing the throughput. This case only occurred in figure 19(b) when the RF $=$ 0%. If there was no turn, the throughput of the VE-mobicast was lower than that of the FAR and mobicast. However, we observed that the average TP of the VE-mobicast $>$ that of the FAR $>$ that of the mobicast, as illustrated in figure 19(a)$\sim$(c). If turns occurred, the throughput of the VE-mobicast was better than that of the FAR and mobicast.

5.2.5 Power consumption ratio (PCR)

Figure 19 shows the simulation results of PCR for the VE-mobicast, mobicast, and FAR. The lower the value of the PCR is, the greater the power savings and longer the network lifetime will be. Figure 20(a) shows the performance of the average PCR vs. various RAs (ranging from 5° to 50°), where 10% $\leq$ the RF $\leq$ 100%, with the ND fixed at 10 nodes/m^2. Figure 20(b) shows the performance of the average PCR vs. various RFs (ranging from 0% to 100%), where 6 $\leq$ ND $\leq$ 20 nodes/m^2, with the RA fixed at 15°. Figure 20(c) shows the performance of the average PCR vs. various NDs (ranging from 6 to 20 nodes/m^2), where 5° $\leq$ RA $\leq$ 50°, with the RF fixed at 50%. The curve of the PCR of the mobicast was higher than that of the FAR, and the curve of the PCR of the FAR was also

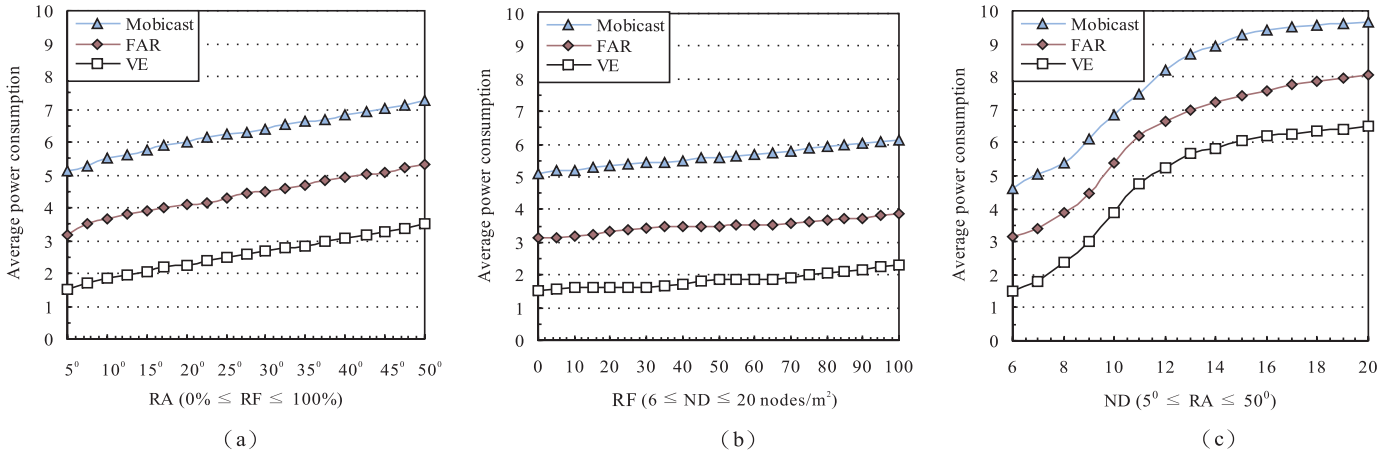

Figure 20: Performance of the average power consumption ratio (PCR) vs. (a) rotation angle (RA), (b) rotation frequency (RF), and (c) network density (ND).

higher than that of the VE-mobicast. The main cost of the PCR for any sensor node is transmitting packets. From figure 20(a)$\sim$(c), the average PCR of the mobicast $>$ that of the FAR $>$ that of the VE-mobicast, because that the total number of transmitted packets of the mobicast $>$ that of the FAR $>$ that of the VE-mobicast.

In summary, our VE-mobicast protocol is a truly efficient routing protocol which achieves high predictive accuracy, a low packet overhead ratio, and a low power consumption ratio.

6 Conclusions

In this paper, we present a new ”spatiotemporal multicast” protocol for supporting applications which require spatiotemporal coordination in a sensornet. To consider the path of a mobile entity which includes turns, in this paper, we develop a new mobicast routing protocol, called the variant-egg-based mobicast (VE-mobicast) routing protocol, by utilizing an adaptive variant-egg shape for the forwarding zone to achieve high predictive accuracy. The main results of the VE-mobicast routing protocol are summarized as follows: (1) the VE-mobicast protocol builds a new adaptive and dynamic shape for the forwarding zone, called the variant-egg, to adaptively determine the size, shape, and location of the forwarding zone in order to maintain the least number of awake sensor

nodes; (2) the VE-mobicast protocol is a fully distributed algorithm which effectively reduces the communication overhead of constructing the forwarding zone and the mobicast message forwarding overhead; (3) the VE-mobicast routing protocol offers high predictive accuracy of forwarding zones. Finally, a mathematical analysis was given, and the simulation results illustrated the performance achievements compared to existing mobicast routing protocols. Future work involves developing a multi-VE-mobicast routing protocol which supports applications of multiple mobile sink nodes in a sensornet.

7 Acknowledgments

This research was supported by the National Science Council of the R.O.C. under grants NSC-92-2213-E-194-022 and NSC-94-2213-E-194-030. This paper is an extension of results presented at IEEE International Conference on Communications, 2005 (ICC 2005). The authors would like to thank the anonymous referees for carefully reading an earlier version of this paper and giving many helpful suggestions.

References

[1] I. F. Akyildiz, W. Su, Y. Sankarasubramaniam, and E. Cayirci. "A Survey on Sensor Networks". *IEEE Communications Magazine*, 40:102–114, August 2002.

[2] P. Bauer, M. Sichitiu, R. Istepanian, and K. Premaratne. "The Mobile Patient: Wireless Distributed Sensor Networks for Patient Monitoring and Care". *Proceedings of the IEEE Conference on Information Technology Applications in Biomedicine (ITAB)*, pages 17–21, November 2000.

[3] J. Boleng, T. Camp, and V. Tolety. "Mesh-based Geocast Routing Protocols in an Ad Hoc Network". *Proceedings of the IEEE International Parallel and Distributed Processing Symposium on Wireless Networks and Mobile Computing (IPDPS)*, pages 184–193, April 2001.

[4] P. Bose and P. Morin. "An Imporved Algorithm for Subdivision Traversal without Extra Storage". *International Journal of Foundations of Computer Science*, pages 297–308, 2002.

[5] P. Bose, P. Morin, I. Stojmenovic, and J. Urrutia. "Routing with Guaranteed Delivery in Ad Hoc Wireless Networks". *ACM Wireless Networks*, 3(4):609–616, 2001.

[6] A. Cerpa, J. Elson, D. Estrin, L. Girod, M. Hamilton, and J. Zhao. "Habitat Monitoring: Application Driver for Wireless Communications Technology". *Proceedings of IEEE Special Interest Group on Data Communication (SIGCOMM)*, pages 20–41, April 2001.

[7] Benjie Chen, Kyle Jamieson, Hari Balakrishnan, and Robert Morris. ”Span: An Energy-Efficient Coordination Algorithm for Topology Maintenance in Ad Hoc Wireless Networks”. *Proceedings of ACM International Conference on Mobile Computing and Networking (MobiCom)*, pages 85–96, July 2001.

[8] Q. Fang, F. Zhao, and L. Guibas. ”Lightweight Sensing and Communication Protocols for Target Enumeration and Aggregation”. *Proceedings of the ACM International Symposium on Mobile Ad Hoc Networking and Computing (MobiHoc)*, pages 165–176, June 2003.

[9] J. L. Gao. ”An Adaptive Network/Routing Algorithm for Energy Efficient Cooperative Signal Processing in Sensor Networks”. *Proceedings of the IEEE Aerospace Conference*, 3:1117–1124, March 2002.

[10] Q. Huang, C. Lu, and G.-C. Roman. ”Spatiotemporal Multicast in Sensor Networks”. *Proceedings of the ACM Conference on Embedded Networked Sensor Systems (SenSys)*, pages 205–217, November 2003.

[11] Q. Huang, C. Lu, and G.-C. Roman. ”Design and Analysis of Spatiotemporal Multicast Protocols for Wireless Sensor Networks”. *Telecommunication Systems, Special Issue on Wireless Sensor Networks*, 26(2-4):129–160, August 2004.

[12] Q. Huang, C. Lu, and G.-C. Roman. ”Reliable Mobicast via Face-Aware Routing”. *Proceedings of the IEEE International Conference on Computer Communications (INFOCOM)*, March 2004.

[13] C. Intanagonwiwat, R. Govindan, D. Estrin, J. Heidemann, and F. Silva. ”Directed Diffusion for Wireless Sensor Networking”. *IEEE/ACM Transactions on Networking*, 11(1):2–16, February 2003.

[14] Y. Ko and N. Vaidya. ”Geocasting in Mobile Ad Hoc Networks: Location based Multicast Algorithms”. *Proceedings of the IEEE Workshop on Mobile Computing Systems and Applications (WMCSA)*, pages 101–110, February 1999.

[15] Y.-B. Ko and N. H. Vaidya. ”GeoTORA: A Protocol for Geocasting in Mobile Ad Hoc Networks”. *Proceedings of the IEEE International Conference on Network Protocols (ICNP)*, pages 14–17, November 2000.

[16] M. Kochhal, L. Schwiebert, and S. Gupta. ”Role-based Hierarchical Self Organization for Wireless Ad Hoc Sensor Networks”. *Proceedings of the ACM international Conference on Wireless Sensor Networks and Applications (WSNA)*, pages 98–107, September 2003.

[17] G. Kulkarni, C. Schurgers, and M. Srivastava. ”Dynamic Link Labels for Energy-Efficient MAC Headers in Wireless Sensor Networks”. *Proceedings of IEEE Sensors*, 2:1520–1525, June 2002.

[18] W.-H. Liao, Y.-C. Tseng, K.-L. Lo, and J.-P. Sheu. ”Geogrid: A Geocasting Protocol for Mobile Ad Hoc Networks Based on Grid”. *Journal of Internet Technology*, 1(2):23–32, December 2000.

[19] J. Liu, J. Reich, and F. Zhao. ”Collaborative In-Network Processing for Target Tracking”. *EURASIP Journal on Applied Signal Processnig*, 4:378–391, 2003.

[20] M. Maleki and M. Pedram. ”Lifetime-Aware Multicast Routing in Wireless Ad Hoc Networks”. *Proceedings of the IEEE Wireless Communications and Networking Conference (WCNC)*, 3:1317–1323, March 2004.

[21] M. Mauve, A. Widmer, and H. Hartenstein. ”A Survey on Position-Based Routing in Mobile Ad Hoc Networks”. *IEEE Network Magazine*, 1:30–39, November 2001.

[22] S. Mishra and A. Nasipuri. ”An Adaptive Low-Power Reservation-Based MAC Protocol for Wireless Sensor Networks”. *Proceedings of the International Performance, Computing, and Communications Conference (IPCCC)*, pages 15–17, April 2004.

[23] J. C. Navas and T. Imielinski. ”Geocast-Geographic Addressing and Routing”. *Proceedings of ACM International Conference on Mobile Computing and Networking (MobiCom)*, pages 66–76, September 1997.

[24] G. Pei and C. Chien. ”Low Power TDMA in Large Wireless Sensor Networks”. *Proceedings of the of Military Communications Conference (MILCOM)*, pages 347 –351, October 2001.

[25] K. Premaratne, J. Zhang, and M. Dogruel. ”Location Information-Aided Task-Oriented Self-Organization of Ad-Hoc Sensor Systems”. *IEEE Sensors Journal*, 4(1):85–95, February 2004.

[26] K. Sohrabi, J. Gao, V. Ailawadhi, and G.J. Pottie. ”Protocols for Self-Organization of a Wireless Sensor Network”. *IEEE Personal Communications*, 7(5):16–27, October 2000.

[27] Y.-C. Tseng, S.-P. Kuo, H.-W. Lee, and C.-F. Huang. ”Location Tracking in a Wireless Sensor Network by Mobile Agents and Its Data Fusion Strategies”. *The Computer Journal*, 47(4):448–460, July 2004.

[28] S.-Y. Wang. ”NCTUns 2.0 Network Simulator and Emulator”. *Network and System Laboratory, Department of Computer Science, National Chiao Tung University (NCTU), Taiwan, http://nsl10.csie.nctu.edu.tw/*.

[29] Eric W. Weisstein. Cassini ovals. *From MathWorld. A Wolfram Web Resource. http://mathworld.wolfram.com/CassiniOvals.html*.

[30] H. Yang and B. Sikdar. ”A Protocol for Tracking Mobile Targets Using Sensor Networks”. *Proceedings of the IEEE Workshop on Sensor Network Protocols and Applications*, pages 71–81, May 2003.

[31] O. Younis and S. Fahmy. ”HEED: A Hybrid, Energy-Efficient, Distributed Clustering Approach for Ah Hoc Sensor Networks”. *IEEE Transaction on Mobile Computing*, 3(4):366–379, October 2004.

[32] M. A. Youssef, M. F.Younis, and K. A. Arisha. ”A Constrained Shortest-Path Energy-Aware Routing Algorithm for Wireless Sensor Networks”. *Proceedings of the IEEE Wireless Communications and Networking Conference (WCNC)*, 2:17–21, March 2002.